AEDC-TR-66-10

C 4

RESULTS OF AN EXPERIMENTAL INVESTIGATION OF THE PERFORMANCE OF AN EXPANSION TUBE

By
Glenn D. Norfleet, John J. Lacey, Jr.,
and Jack D. Whitfield
ARO, Inc.

February 1966

Distribution of this document is unlimited.

VON KÁRMÁN GAS DYNAMICS FACILITY
ARNOLD ENGINEERING DEVELOPMENT CENTER
AIR FORCE SYSTEMS COMMAND
ARNOLD AIR FORCE STATION, TENNESSEE

NOTICES

When U. S. Government drawings specifications, or other data are used for any purpose other than a definitely related Government procurement operation, the Government thereby incurs no responsibility nor any obligation whatsoever, and the fact that the Government may have formulated, furnished, or in any way supplied the said drawings, specifications, or other data, is not to be regarded by implication or otherwise, or in any manner licensing the holder or any other person or corporation, or conveying any rights or permission to manufacture, use, or sell any patented invention that may in any way be related thereto.

Qualified users may obtain copies of this report from the Defense Documentation Center.

References to named commercial products in this report are not to be considered in any sense as an endorsement of the product by the United States Air Force or the Government.

RESULTS OF AN EXPERIMENTAL INVESTIGATION OF THE PERFORMANCE OF AN EXPANSION TUBE

Glenn D. Norfleet, John J. Lacey, Jr.,
and Jack D. Whitfield

ARO, Inc.

AF - AEDC
Arnold AFS Tenn

FOREWORD

The research reported herein was done by ARO, Inc. (a subsidiary of Sverdrup and Parcel, Inc.), contract operator of the Arnold Engineering Development Center (AEDC), Air Force Systems Command (AFSC), Arnold Air Force Station, Tennessee, under Contract AF 40(600)-1200. The tests were conducted from July 3, 1963 through January 29, 1965 under ARO Project No. VJ2604. The Program Element was 62410034, the Project 7778, and the Task 777806.

This information contained in this report was presented as a paper at the Fourth Hypervelocity Techniques Symposium held at Arnold Air Force Station, Tennessee, November 15-16, 1965. The manuscript was submitted for publication on December 17, 1965.

This technical report has been reviewed and is approved.

A. G. Williams
Project Engineer
Technology Division
DCS/Plans and Technology

Donald D. Carlson
Colonel, USAF
DCS/Plans and Technology

ABSTRACT

The results from an experimental study of an expansion tube conducted at the von Karman Gas Dynamics Facility (VKF) are presented and discussed. The research was conducted in two facilities: (1) a 6.75-in.-diam Modified Expansion Tube (MET) which utilizes a partially steady and partially unsteady expansion process, and (2) a 4-in.-diam (constant diameter) High Density Shock Tube (HDST) operated in an expansion tube mode for a completely unsteady expansion of the shock-heated gas to the final test condition. Flow velocities from approximately 9000 to 16,000 ft/sec were studied. The theoretical performance of expansion tubes in terms of velocity is found to be nearly obtained; however, the steadiness of the resulting flow leaves much to be desired, and the definition of accurate flow conditions remains in serious doubt.

CONTENTS

		Page
	ABSTRACT	iii
	NOMENCLATURE	viii
I.	INTRODUCTION	1
II.	DISCUSSION	2
III.	APPARATUS	
	3.1 AEDC-VKF Modified Expansion Tube	3
	3.2 AEDC-VKF High Density Shock Tube	4
	3.3 Models	5
	3.4 Instrumentation	5
IV.	EXPERIMENTAL RESULTS	
	4.1 Pitot-Pressure Disturbances	6
	4.2 Performance Data	11
V.	CONCLUSIONS	14
	REFERENCES	15

ILLUSTRATIONS

Figure		
1.	Comparison of Expansion Tube and Shock Tunnel	17
2.	Proximity of Test Gas to Secondary Diaphragm - Expansion Tube	17
3.	Wave Diagram - Schematic	18
4.	Variation of Performance and Test Slug Length with Area Ratio	19
5.	AEDC-VKF Modified Expansion Tube	20
6.	Altitude-Velocity Regime, Modified Expansion Tube	21
7.	Modified Expansion Tube - Flow Properties, "Standard Conditions"	22
8.	Constant Area Tube Installation - Schematic	23
9.	AEDC-VKF High Density Shock Tube	24
10.	High Density Shock Tube - Flow Properties (P_8 = 16 μHg)	25
11.	Models - Modified Expansion Tube	26
12.	Pitot Rake - High Density Shock Tube	27

Figure		Page
13.	Sketch of Rake and Sample Pitot Pressure - 6.75-in. Modified Expansion Tube	28
14.	Typical Pitot Traces for a Flat Face Cylinder Model	29
15.	Typical Pitot Traces for a Hemisphere-Cylinder Model	30
16.	Pitot Rake Traces - Two Different Accelerating Tube Lengths	31
17.	Typical Traces for a Centerline Pitot Probe	32
18.	Typical Pitot Traces for Helium-Air Mixture Accelerating Gas (Hemisphere-Cylinder Model)	33
19.	Pitot and Static Pressure Traces, d_8 = 6.75 in., One 3/4-mil Polyester	34
20.	Pitot and Static Pressure Traces, d_8 = 6.75 in., One 3/4-mil Aluminum Foil	35
21.	Monochromatic (≈3090 Å) Radiation Using Aluminum Foil and Polyester Secondary Diaphragm	36
22.	Pitot Pressure Traces, d_8 = 1.60 in., One 3/4-mil Polyester	37
23.	Comparison of Flush and Recessed Mounting of Pressure Transducer	38
24.	Sketch of Rake and Sample Pitot Pressure Traces High Density Shock Tube, P_8 = 16 μHg	39
25.	Sketch of Rake and Sample Pitot Pressure Traces High Density Shock Tube, P_8 = 100 μHg	40
26.	Sketch of Rake and Sample Pitot Pressure Traces High Density Shock Tube, P_8 = 18 mm Hg	41
27.	Accelerating Tube Shock Velocity - Modified Expansion Tube	42
28.	Accelerating Tube Shock Velocity - High Density Shock Tube	43
29.	Driven Tube Shock Velocity - Modified Expansion Tube	44
30.	Driven Tube Shock Velocity - High Density Shock Tube	45
31.	Pitot Pressure at the Test Section	46
32.	Pitot Pressure Profile - Modified Expansion Tube	47

Figure		Page
33.	Pitot Pressure Profile - High Density Shock Tube	48
34.	Static Pressure Measurements	49
35.	Wall Static Pressure at the Test Section	50
36.	Measured Pitot and Wall Static Pressure Compared with Theory - Modified Expansion Tube	51
37.	Measured Pitot and Wall Static Pressure Compared with Theory - High Density Shock Tube	52
38.	Shock Heated Gas Passage Time, t_7	53
39.	Shock-Interface Separation	54

TABLES

I.	Instrumentation	55
II.	Spike Hypotheses	56

NOMENCLATURE

A	Cross-sectional area of tube
a	Acoustic speed
d	Inside diameter of tube
h	Enthalpy
ℓ_1, ℓ_4, ℓ_8	Tube lengths (see Fig. 3)
ℓ_t	Test gas slug length at time of rupture of secondary diaphragm
M	Mach number
M_s	Shock Mach number
P	Pressure
P'_o	Pitot pressure
P_{HCW}	Hemisphere-cylinder wall static pressure
r	Radial distance from tube centerline
T	Temperature
t	Time
U	Velocity
U_s	Shock velocity
x	Axial distance
γ	Ratio of specific heats
ρ	Gas density
τ	Ideal test time from inviscid simple shock-tube theory

SUBSCRIPTS

1, 2, 2a, 3, etc.	Denotes various regions in shock tube flow (see Fig. 3)
o	Stagnation conditions
∞	Free-stream conditions

DUAL SUBSCRIPTS

Denotes ratio of quantities, example:

$$P_{ij} \equiv P_i/P_j$$

SECTION I
INTRODUCTION

The present need for advancement of ground test facilities for hypervelocity flow research is quite apparent from even a cursory survey of the attendant problems. A recent extensive survey paper by Cheng (Ref. 1) discusses many of these problems. The spectra of hypervelocity flow problems is indeed quite wide, and many different types of aerodynamic tools will be required to cover the ever-increasing domain of velocities and altitudes.

An aerodynamic test device utilizing an unsteady expansion to accelerate shock-heated gas was apparently first proposed by Resler and Bloxsom (Ref. 2) and was treated briefly by Hertzberg, et al. (Ref. 3). Trimpi (Ref. 4) was the first to make a detailed theoretical study of the expansion tube, i. e., a device in which the entire expansion from the shock-heated condition to the final test condition is performed unsteadily. The theoretical advantage of an unsteady expansion in hypersonic flow is evident from comparison of the steady and unsteady equations for isentropic expansions of the testing medium. For a steady expansion,

$$dU = -(dh/U)$$

whereas for an unsteady expansion,

$$dU = -(dh/a)$$

Thus, for hypersonic testing ($U \gg a$, $M \gg 1$) the unsteady expansion yields a velocity increment M times the steady expansion for a given incremental reduction in static enthalpy. It has been shown (Ref. 4) that for a given density level the test gas velocity obtainable with an expansion tube is approximately double that obtained by the shock tunnel for the same enthalpy level. Such a comparison is shown in Fig. 1.

Trimpi (Ref. 4) discussed both known and anticipated advantages and disadvantages of the expansion tube concept. One of the anticipated difficulties Trimpi mentioned is the fact that only an extremely small portion of the shock-heated gas is used for test purposes. Some insight into the problem can be gained from Fig. 2, which shows that for the expansion tube all of the shock-heated gas (air) used for test purposes

is in very close proximity to the secondary diaphragm at the time of its rupture.

A modification* of the expansion tube concept is proposed herein to alleviate the test gas slug length problem, and experimental data from both modified and normal expansion tubes are presented and discussed.

SECTION II
DISCUSSION

The purpose of this investigation is to assess the value of an expansion tube as a hypervelocity aerodynamic test device. Flow uniformity is, of course, of major importance in aerodynamic testing, and because of the close proximity of the test gas to the rupturing secondary diaphragm, was of major concern in this investigation. To this end it was decided to investigate a modified version of the expansion tube designed to alleviate this problem.

The modification consisted of the addition of an area change (a supersonic nozzle) between the driven and the accelerating tubes (see Fig. 3). The shock-heated gas is expanded first by a steady expansion to the 2a conditions (Fig. 3) and then by an unsteady expansion to the test conditions (region 6).

The major advantage of such a modification is that there is a significant increase in the length to diameter ratio of the test slug, ℓ_t/d_1, at diaphragm rupture and, hopefully, a corresponding increase in test gas uniformity. The major disadvantage is a decrease in performance due to the use of a partially steady expansion versus a completely unsteady expansion. This performance loss is shown as a function of area ratio in Fig. 4. (Note that the velocity parameter, $U_\infty/\sqrt{2h_{o2} - 2h_\infty}$ is a "coefficient of performance", i.e., it represents the gain in performance by the use of the unsteady expansion.) By using a nozzle with an area ratio of 10, the length parameter, ℓ_t/d_1, is increased by over an order of magnitude while the "coefficient of performance" is decreased to about 1.5 for the cases considered herein, which represents a velocity loss of about twenty-five percent due to the steady expansion.

The idealized run time of a modified expansion tube with an abrupt area change is equal to that of a normal

*Such a modification is discussed briefly by Hertzberg, et al. (Ref. 3).

expansion tube of the same length and test gas conditions. For a modified tube with a nozzle of finite length, the actual run time will be reduced by the nozzle start time and will depend upon the specific nozzle configuration.

During the course of this investigation, a question arose as to the effects of the nozzle itself on the test gas uniformity. An investigation was then undertaken in a 4-in.-diam buffered shock tube (the AEDC-VKF High Density Shock Tube - HDST). The tube was run as a normal expansion tube. Some experimental results are presented for this expansion tube as well as the modified version.

SECTION III
APPARATUS

3.1 AEDC-VKF MODIFIED EXPANSION TUBE

The AEDC-VKF Modified Expansion Tube (MET) is shown in Fig. 5. The driver is 11 in. long with a 2.89-in. I.D. The driven section is 82 in. long and has a 1.58-in. diameter. A transition section (nozzle) between the driven and accelerating sections is 50 in. long. Its design will be discussed in the next paragraph. The accelerating section is 42-ft long and has a 6.75-in. diameter. An open-jet test section (15 in. in diameter by 2 ft long) is used and a 2-ft-diam by 12-ft-long dump tank completes the facility.

The area ratio, A_{8_1}, for this facility is 18.3, and the nozzle was designed by the method of Shapiro (Ref. 5). This is a sophisticated fairing procedure and does not rely on wave cancellation. Therefore, the design is not as sensitive to boundary-layer displacement thickness (δ^*) as the method of characteristics. Use of this method is based on the indication of Ref. 6 that it produces a shockless nozzle and the flow downstream is reasonably free of disturbances. For an initial shock Mach number $M_{s_1} = 6.9$ into 0.55-atm air, the nozzle entrance Mach number (M_2) = 2.12 and exit Mach number (M_{2_a}) = 4.75. The boundary-layer displacement thickness was estimated to be very thin, and no correction was made for it. Real gas properties of Refs. 7 and 8 were used to calculate conditions throughout the entire flow process. The parameter μ of Ref. 5 was chosen to be 8.25, and the nozzle exit angle is 0.08 deg. The resulting nozzle is a 7-deg half-angle cone with a diameter from 1.58 to 5.80 in. and a smooth contour from the latter dimension to 6.75 in. in diameter.

As was previously mentioned, the run time of a modified expansion tube is reduced by the nozzle start time. This start time is that time required for the head of the unsteady expansion to be swept through the nozzle. The start time for the MET nozzle is not accurately known. It is estimated that the start time for "standard"* run conditions is nearly equal to the ideal run time. However, for most of the start time, the head of the unsteady expansion is in the contoured portion of the nozzle where the cross-sectional area is approximately equal to that of the accelerating tube. The effective nozzle start time is then somewhat less than actual start time, and probably leaves an appreciable run time, disregarding all other test-time loss mechanisms.

The MET operating regime is shown in Fig. 6 based on using room temperature (300°K) helium as the driver gas at a pressure of 1700 atm. The calculations are based upon ideal one-dimensional flow with no losses. Most runs were made at the "standard" condition, duplication altitude $\approx$ 125,000 ft and $U_\infty \approx$ 14,000 ft/sec. Theoretical gas properties in regions of interest are shown for the "standard" shot in Fig. 7.

In addition to the "standard" shot, the following special conditions were run:

1. reduced driver pressure,
2. increased accelerating tube pressure,
3. helium-air mixtures were used as the accelerating gas, and
4. by adding a small tube inside the accelerating tube (see Fig. 8) runs were made in the constant-area expansion tube mode.

3.2 AEDC-VKF HIGH DENSITY SHOCK TUBE

The AEDC-VKF High Density Shock Tube (HDST) shown in Fig. 9 was used for experiments of the unmodified concept. It is a 112-ft-long, constant, 4-in.-diam tube, 18 ft of which is the driver. The remaining 94 ft can be sectioned by diaphragms at various locations as desired. For these experiments the driven length is 64 ft, and the accelerating section is 18 ft long, with 12 ft remaining to allow for shock reflection.

The driver and driven tube charge conditions were held constant for all runs with room temperature ($\approx$ 300°K) gases

*See Fig. 7 for "standard" shot conditions. Duplication altitude conditions based on U. S. Standard Atmosphere 1962 (Ref. 16).

used throughout:

$$P_4 = 680 \text{ atm} -- \text{helium}$$
$$P_1 = 259 \text{ mm Hg} -- \text{air}$$

The accelerating gas was air for all runs and the charge pressure (P_8) was varied from 16 μHg to 18 mm Hg. Theoretical gas conditions in the regions of interest are presented in Fig. 10 for the case of $P_8 = 16$ μHg.

3.3 MODELS

Several models (Fig. 11) were used in the MET phase of the tests. The hemisphere-cylinder and flat-faced cylinder were mounted on tube centerline and tested only at $\ell_8 = 46$ ft (i.e., the test section). The pitot rake and the single pitot probe were tested at several longitudinal stations.

The pitot rake used in the HDST phase is shown in Fig. 12. The piezoelectric transducers were mounted in the recessed manner shown to protect the transducer from any large particles that might be in the flow. All tests in the HDST were made with the rake at $\ell_8 = 18$ ft.

3.4 INSTRUMENTATION

Pressure and shock velocity measurements were made in these tests. Table I presents the instrumentation used and pertinent data. Transducer sensitivity, rise time, and filter configuration varied throughout the tests, and the values given in Table I are approximate.

For pitot pressure measurements, the transducer output caused by aerodynamic heating was found to be of the same order of magnitude as the pressure signal. It was determined that the transducer could be thermally protected by the application of a rubber mastic "gage kote" to the sensing surface. The application of this thermal shield did not change the transducer sensitivity or response time appreciably.

The monochrometer and photomultiplier setup consisted of a 2000 to 14,000 Å monochrometer set for a resolution of approximately 100 Å with a photomultiplier tube of unknown sensitivity placed at the exit slit. An approximate wavelength calibration was made by scanning the spectra of a neon indicator lamp. The entrance slit and associated lens were used to focus on an area approximately 0.1 in. square at the

nose of the hemisphere-cylinder. The output of the photomultiplier tube was recorded on an oscilloscope.

SECTION IV
EXPERIMENTAL RESULTS

Early results in the modified expansion tube yielded pitot-pressure measurements which indicated the presence of strong timewise disturbances in the test gas. These disturbances, or "spikes", were found to be most pronounced on the tunnel centerline as can be seen in Fig. 13. The major effort of this investigation was directed toward the determination of the origin of these spikes. Runs were not made over a wide range of test gas conditions and most runs were made at the "standard" conditions listed in Fig. 7. Since the major point of interest was a timewise variation in test gas conditions, no great care was taken to insure the accuracy of the absolute level of the pressure measurements. There are some runs in which absolute value of pitot pressure and wall static pressure were measured to a reasonable accuracy and experimental results from these runs are presented and discussed in Section 4.2.

4.1 PITOT PRESSURE DISTURBANCES

The basic approach taken in the search for the origin of the spikes was:

1. hypothesize an agent which might cause the spike,
2. vary the apparent controlling parameter while holding others constant, and
3. look for changes in the nature of the spike greater than the normal run-to-run variation.

The various hypotheses and the parameteric variations accomplished to test the hypotheses are listed in Table II. The results are discussed below.

4.2.1 Hypothesis I – Mechanically Induced Accelerations

Since the pressure transducers are very sensitive to acceleration normal to the sensing diaphragm, the possibility exists that the spikes are mechanically induced. This possibility was ruled out by making large changes in model and support system without effecting the character of the spikes.

4.1.2 Hypothesis II – Instrumentation Difficulties

The possibility that the spikes were somehow generated by the pressure transducer and/or the associated electronic circuitry was considered. A pitot rake (Fig. 11c) was used to observe five pitot pressures simultaneously. These data (Fig. 13) show that the spikes are predominant on the tube centerline. A further check was made by completely interchanging the centerline and an off-axis instrument channel, and subsequent runs show the spikes to remain predominately on the tube centerline. From these checks and the tests discussed in Section 4.1.1, it was concluded that the spikes were not mechanical or electronic in nature but rather indicated flow disturbances.

4.1.3 Hypothesis III – Flow Instability on Model

The initial indications of spikes were obtained from the flat-faced cylindrical model (Fig. 11b) (typical traces shown in Fig. 14), thus the possibility that the spikes could be induced by some model-flow instability was considered. Smaller diameter, flat-faced probes (e.g., the pitot rake, Fig. 11c) and hemisphere-cylinder (Fig. 11a) models were tested, and typical traces from these tests are shown in Figs. 13 and 15, respectively. The radial location of the models was found, for example, to be far more critical with regard to the character of the spikes than the model configuration.

4.1.4 Hypothesis IV – Oblique Shock from Wall

The fourth hypothesized agent was an oblique shock wave which arrives at the test section approximately on the tunnel centerline. Slight timewise flow variations would lead to movement of the shock across the centerline pitot probe which would cause variations in the centerline pitot pressure, but would not greatly affect the pitot pressure off centerline. A longitudinal pitot survey using either the pitot rake (typical traces shown in Fig. 16) or a single centerline pitot probe (typical traces shown in Fig. 17) indicated that the pitot spikes were present on centerline for all longitudinal stations checked, thus apparently eliminating the oblique shock hypothesis.

4.1.5 Hypothesis V – Accelerating-Tube Viscous Effects

The fifth hypothesis is that the spikes are caused by viscous effects in the accelerating tube. A major constituent of the boundary layer in the accelerating tube is the shock-heated accelerating gas which is normally air. Several runs were made with helium-air mixture as the accelerating gas,

thus changing the boundary-layer constituents, with no noticeable change in the nature of the pitot spikes (typical traces shown in Fig. 18). The small, but finite, normal leakage of room air into the accelerating tube precluded the use of highly pure helium. The helium concentration was varied from sixty-five to ninety percent (by volume).

4.1.6 Hypothesis VI – Secondary Diaphragm Rupture Effects

The secondary diaphragm is a natural suspect for producing the pitot spikes because of the proximity of the test gas to the diaphragm at the time of rupture (for the standard shot $\ell_t \approx 0.84$ in.). To check this possibility, diaphragm thickness was varied from 0.00025 to 0.008 in., and several different materials were used. Figure 19 presents what is considered to be the spread of the data using a 3/4-mil polyester secondary diaphragm. All other diaphragms tested with the exception of the aluminum foil secondary diaphragm yielded pitot traces which appeared to fall within this scatter.

Figure 20 shows the results for the aluminum foil secondary diaphragm. The three traces presented are representative of run-to-run variations. Note that the time scale of the traces of Figs. 19 and 20 are the same and that there is a change in the character of the spikes and no change of the static pressure trace.

4.1.7 Hypothesis VII – Flow Contamination by Secondary Diaphragm

For high Mach number flow,

$$P_o' \approx K \rho U^2 \qquad (1)$$

Pitot spikes could then be caused by steep gradients in density. Gaseous contamination from the secondary diaphragm is one possible source of dense gas. A monochrometer at the test section was used to detect this contamination when an aluminum foil diaphragm was installed. The monochrometer was set to pass narrow bandwidth radiation about a strong aluminum line (3090 Å). Although another aluminum line is stronger, it is near other predominate spectra. The data obtained (Fig. 21) indicate that this contamination arrives during the useful flow but shows no correlation with the pitot disturbances which appear later in the flow. The run with a polyester secondary diaphragm (Fig. 21) served as a "tare" run (i.e., aluminum contamination was not detected). It should be noted that this technique may be insensitive to relatively cool particle contamination.

4.1.8 Hypothesis VIII – Area Change Effect

The AEDC-VKF modified expansion tube makes use of a steady expansion (nozzle) prior to the unsteady expansion. It is questionable that this nozzle actually has time to start during the short run time. In addition, there is a good possibility that some weak shock waves are formed in the turning process although the nozzle is supposedly contoured to eliminate shock formation. It is not obvious how either of these difficulties would result in pitot spikes; however, it is plausible. As a check, a 1.6-in.-diam tube was inserted inside the accelerating tube (Fig. 8), thus eliminating the nozzle. An attempt was made to position a single pitot probe on tube centerline. However, it was necessary to position the pitot probe externally, and it may have been slightly off centerline. The data from this probe (Fig. 22) show no spikes, but the character of the trace cannot be explained. The possibility exists that the tube, which was not exceedingly smooth, was completely filled with boundary layer at the test station.

The results from the constant-area tube were promising, at least in that they showed no pitot spikes, and further study seemed advisable. In order to relax problems inherent with the small diameter tube, the experiment was continued in the AEDC-VKF Pilot High Density Shock Tube (HDST) operated as a constant-area expansion tube. Early runs, while producing little usable aerodynamic data, clearly demonstrated, through several mechanical failures, the high drag loads present during the passage of the unsteady expansion fan.

A second operational problem demonstrated by the constant-area experiment was the hazardous location of transducers with respect to material lost from the rupturing primary diaphragm. For the original runs in the 4-in. expansion tube, the pitot-rake probes were instrumented with flush-mounted transducers as was the case in the MET. After losing several transducers from damage caused by diaphragm particles, it was decided to give the transducers some protection by recessing them into the probe. The specific configuration used along with a comparison of pressure measurement using each mounting technique is shown in Fig. 23. Although the pressure traces are not identical, the recessed gage seems adequate both in terms of response and acoustical ringing of the cavity.

The constant-area experiment was carried out holding the driver and driven tube conditions constant and varying the accelerating tube charge pressure and thus the length of the test gas slug, ℓ_t. (For P_8 = 16 μHg, $\ell_t \approx$ 0.035 in.; for P_8 = 18 mm Hg, $\ell_t \approx$ 7.7 in.)

Typical run traces for runs with low P_8 (and therefore relatively short initial test slug length) are shown in Figs. 24 and 25. Once again, there are large disturbances on the pitot pressure traces. The shape of these disturbances is somewhat different from those observed in MET; however, their relative magnitudes are approximately the same.

Typical run traces for runs with high P_8 (and therefore relatively long test slug length) are shown in Fig. 26. Here, the disturbances occur at a much higher frequency and are of somewhat reduced relative amplitude. Whether the disturbances on these traces are the same phenomena as those at the lower P_8 is a matter of conjecture; however, from continuity considerations it is expected that frequency of the disturbances should decrease as the gas is further expanded. In addition, if the disturbances are density gradients, their amplitude relative to the mean pitot pressure is expected to increase as the ratio of dynamic to static pressure increases. It is possible then, that the disturbances seen on both low and high pressure runs may result from the same basic phenomena but appear different in frequency and amplitude because of the amount of expansion permitted.

It is interesting to compare the pitot pressure trace before and after arrival of the interface. This comparison is shown in Fig. 26 for a case where the pitot pressures before and after the interface are not vastly different. From these traces it is apparent that the uniformity of the shock-heated gas (region 7) is superior to that of the expanded gas (region 6).

Assuming that the disturbances are in some way induced by the secondary diaphragm, it is expected that they should diminish in time since the gas arriving at the test station later in time was further from the secondary diaphragm at the time of rupture. The traces, in fact, show little indication of disturbance attenuation in the available test time. Two diametrically opposed possibilities are apparent:

1. The disturbances are not caused by the secondary diaphragm, or

2. The effects of the secondary diaphragm are so extensive that the entire test slug length was affected to approximately the same degree.

Since the disturbances arrive at the same time as the interface, the first possibility seems somewhat remote.

4.1.9 Summary

Of the many hypotheses tested only two showed any effect on the spikes:

1. Deletion of the area change affects the shape of the disturbances, but disturbances of about the same relative magnitude as that of the MET spikes are present even without an area change.

2. Changes in secondary diaphragm material appreciably changed both the shape and the time of arrival of the spikes but had little effect on their magnitude.

4.2 PERFORMANCE DATA

Although the uniformity of the test gas leaves much to be desired, it is of interest to compare approximate mean levels of the measured data with theoretical predictions.

4.2.1 Velocity

No direct measurement of flow velocity was attempted; however, it can be shown from viscous considerations (Refs. 9, 10 and 11) that the interface velocity (and therefore the test gas velocity at the interface) is approximately equal to the accelerating tube shock velocity, U_{s8}. This shock velocity was found to be slightly below theory at the test section (Figs. 27 and 28), which implies that the flow velocity is in reasonable agreement with theory. The theory is based upon measured values of M_{s1}, P_1, P_8, and one-dimensional inviscid flow using the thermodynamic properties of Ref. 12. The runs represented by the scatter band contain data from all runs in which reasonably reliable absolute pressure measurements were made.

Driven tube shock velocity, U_{s1}, is compared with theory in Figs. 29 and 30. The theory was based upon one-dimensional inviscid flow with no losses. The driver gas, helium, was considered to be perfect, and the driven gas, air, was considered real, using the thermodynamic properties of Ref. 12. The initial shock strength was found to be slightly above theory and for the high P_{41} case in MET, initially increases with time. Both of these phenomena were observed by White (Ref. 13) who attempts to explain them by a "formation from compression" model.

4.2.2 Pitot Pressure

Pitot pressure was measured on all the models shown in Fig. 11. No significant model-to-model variation was found in either level or uniformity of the pitot pressure. To attempt to determine the level of pitot pressure for these runs is perhaps a bit courageous, but it was felt that even an approximate level might be a worthwhile piece of information at this point in expansion tube development.

The MET traces were read at a time, t_1, (Fig. 13) soon after the arrival of the interface but purposely chosen to avoid spikes. For the MET runs with the pitot rake, a second time, t_2, (Fig. 13) was chosen after the rapid decrease in pitot pressure on the two outer probes (apparent arrival of the boundary layer). Once again, the time, t_2, was chosen to avoid spikes. The HDST traces were read at a time t_1 (Fig. 24) immediately after the arrival of the interface, and here the pressure level was determined by fairing through the disturbances.

Measured centerline pitot pressures are compared with theory in Fig. 31. The theoretical calculations are based upon:

1. Measured U_{s_1} and P_1 (T_1 assumed to be room temperature)
2. Normal shock crossings using the thermodynamic properties of Refs. 12 and 13 to determine conditions in region 2.
3. Isentropic expansion of the gas in region 2 to $U_6 = U_{s_8(\text{measured})}$ using the properties of Refs. 12 and 13.
4. A steady isentropic expansion (for MET) calculated from the geometric area ratio, i.e., zero boundary-layer displacement thickness.

The estimated overall accuracy in measured P_o' is ±12%. The measured pitot pressure is in reasonable agreement with theory for the low velocity runs, but is considerably below theory for the higher velocity runs. It should be remembered that the higher velocity runs have a stronger unsteady expansion fan and a lower pitot pressure.

Observed pitot pressure profiles in MET are shown in Fig. 32. As previously stated, the two times, t_1 and t_2, are before and after the apparent arrival of the boundary layer

at the two outer pitot probes. Pitot profiles from the HDST are shown in Fig. 33. A rapid decrease in pitot pressure on the outer pitot probes corresponding to that observed in MET was not found. Theory in both cases was calculated as previously described.

4.2.3 Wall Static Pressure

Typical oscilloscope traces of the wall static pressure measurements are shown in Fig. 34. The "dip" in static pressure from the MET runs is typical and, like the spikes, is yet to be explained. The results of the static pressure measurements are shown in Fig. 35. The MET traces were read at the same point in time, t_1, as on the pitot trace. The estimated accuracy is ±17%. Here again, the measured pressure is in fair agreement with the theory for low velocity runs but is considerably low for the higher velocities. The theoretical free-stream static pressure was calculated using the same assumptions listed for the calculations of $P_{o_{theory}}$.

Reliable pitot pressure and wall static pressure were obtained concurrently in only six runs - three in MET at low pressures and three in HDST at high pressure. The measurements are compared to theory in Figs. 36 and 37. The theory was obtained as described previously except that the gas in region 2 is expanded to a given P_6, whereas previously it was expanded to a given U_6 (= U_{s8}). The results agree reasonably well with theory for both the high pressure and low pressure runs. This could be anticipated from the previous comparisons since both pitot and wall static pressure were in agreement with theory at high pressure and both low at low pressure. It should be noted here, that the theoretical velocities, U_6, obtained by expanding to $P_{6(measured)}$ are approximately 7 percent higher than the experimentally observed U_{s8} values for MET (Fig. 36). For the HDST (Fig. 37) the only data presented are for higher pressures, and here the theoretical velocity, U_6, is slightly less than $U_{s8(measured)}$.

4.2.4 Shock-Interface Separation

The separation time between the shock and the apparent interface can be determined from the pitot pressure trace. This time is compared to the theory of Mirels (Refs. 10 and 11) as a function of P_8 in Fig. 38. For low P_8 the spread of the data becomes large and the agreement with theory becomes poor.

Shock and interface curvature was obtained by determining their time of arrival at each probe of the pitot rake

in MET. The time scale was expanded for several runs in order to increase the experimental accuracy. Results of these runs are presented in Fig. 39. The rise time of the pressure transducer precluded very accurate measurements of shock curvature; however, the results are in reasonable agreement with those of Ref. 14. The curvature of the interface was so severe that the transducer rise time was comparatively insignificant. Also the large scatter in t_7 (Fig. 38) is seen here as a run-to-run variation in the separation distance.

SECTION V
CONCLUSIONS

Based on the results of this experimental study of an expansion tube, the following conclusions are made:

1. Expansion tube performance in terms of shock velocity and, therefore presumably flow velocity, is in reasonable agreement with theoretical predictions.

2. Pitot pressure measurements on centerline indicate flow disturbances of sufficient magnitude to preclude meaningful aerodynamic testing during these disturbances. No firm conclusions can be drawn as to the source of these disturbances; however, the present results point to the secondary diaphragm as the possible source of these disturbances.

3. A brief test time can be chosen such that both wall static and pitot pressures are fairly constant in time; however, during this time both pressures are somewhat lower than expected based upon measured shock velocities, and thus the definition of accurate test conditions during even this time remains in serious doubt.

REFERENCES

1. Cheng, H. K. "Recent Advances in Hypersonic Flow Research." AIAA Journal, Vol. 1, No. 2, February 1963, pp. 295-310.

2. Resler, E. L. and Bloxsom, D. E. "Very High Mach Number Flows by Unsteady Flow Principles." Cornell University, Graduate School of Aeronautical Engineering, January 1952.

3. Hertzberg, A., Smith, W. E., Glick, H. S., and Squire, W. "Modifications of the Shock Tube for the Generation of Hypersonic Flow." AEDC-TN-55-15, March 1955.

4. Trimpi, Robert L. "A Preliminary Theoretical Study of the Expansion Tube, A New Device for Producing High-Enthalpy Short-Duration Hypersonic Gas Flows. NASA TR R-133, 1962.

5. Shapiro, A. H. "Nozzles for Supersonic Flow without Shock Fronts." Journal of Applied Mechanics, Vol. 11, No. 2, June 1944, pp. A93-100.

6. Keenan, J. H. and Neumann, E. P. "Friction in Pipes at Supersonic and Subsonic Velocities." NACA TN-963, January 1945.

7. Hilsenrath, J., Klein, M., and Woolley, H. W. "Tables of Thermodynamic Properties of Air Including Dissociation and Ionization from 1500°K to 15,000°K." AEDC-TR-59-20 (AD 229962), December 1959.

8. Lewis, C. H. and Burgess, E. G. "Empirical Equations for the Thermodynamic Properties of Air and Nitrogen to 15,000°K." AEDC-TDR-63-138 (AD 411624), July 1963.

9. Roshko, Anatol. "On Flow Duration in Low-Pressure Shock Tubes." Physics of Fluids, Vol. 3, No. 6, November-December 1960, pp. 835-842.

10. Mirels, H. "Test Time in Low-Pressure Shock Tubes." Physics of Fluids, Vol. 6, No. 9, September 1963, pp. 1201-1214.

11. Mirels, H. "Shock Tube Test Time Limitation Due to Turbulent-Wall Boundary Layer." AIAA Journal, Vol. 2, No. 1, January 1964, pp. 84-93.

12. Hilsenrath, J. and Klein, M. "Tables of Thermodynamic Properties of Air in Chemical Equilibrium Including Second Virial Corrections from 1500°K to 15,000°K." AEDC-TDR-63-161 (AD 416040), August 1963.

13. Humphrey, R. L. and Neel, C. A. "Tables of Thermodynamic Properties of Air from 90 to 1500°K." AEDC-TR-61-103 (AD 262692), August 1961.

14. White, D. R. "Influence of Diaphragm Opening Time on Shock Tube Flows." Journal of Fluid Mechanics, Vol. 4, Part 6, November 1958, pp. 585-599.

15. Liepmann, H. W. and Bowman, R. M. "Shape of Shock Fronts in Shock Tubes." The Physics of Fluids, Vol. 7, December 1964, pp. 2013-2015.

16. U. S. Standard Atmosphere, 1962. U. S. Government Printing Office, Washington, D. C., December 1962.

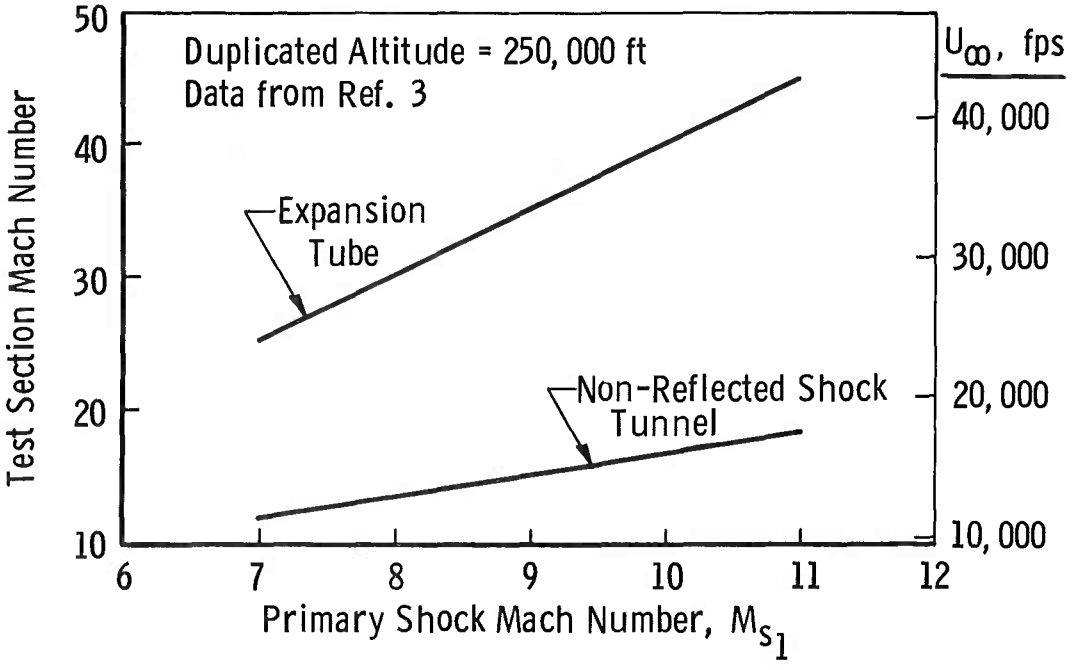

Fig. 1 Comparison of Expansion Tube and Shock Tunnel

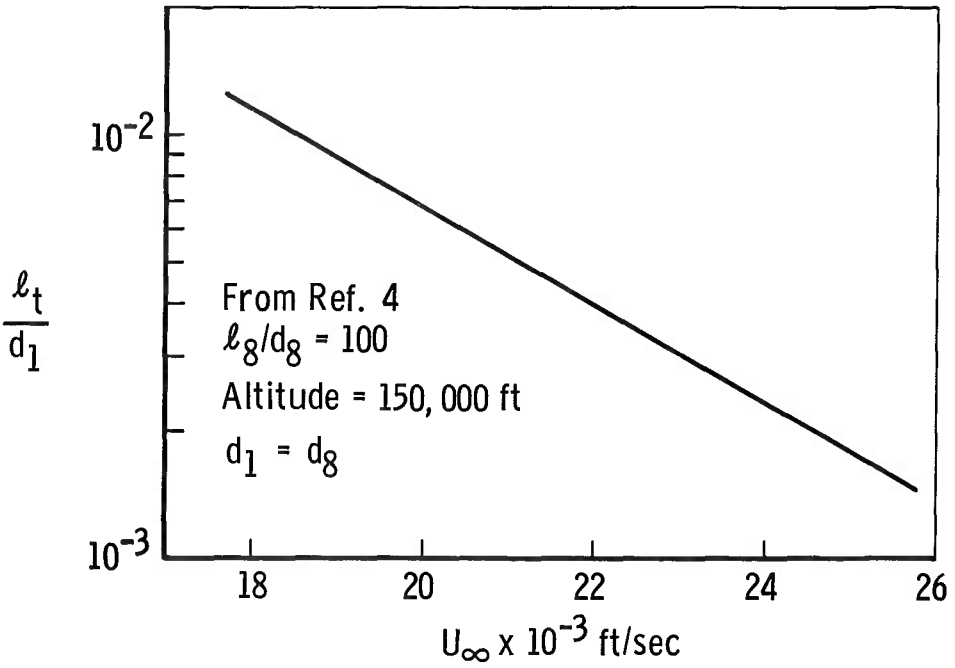

Fig. 2 Proximity of Test Gas to Secondary Diaphragm – Expansion Tube

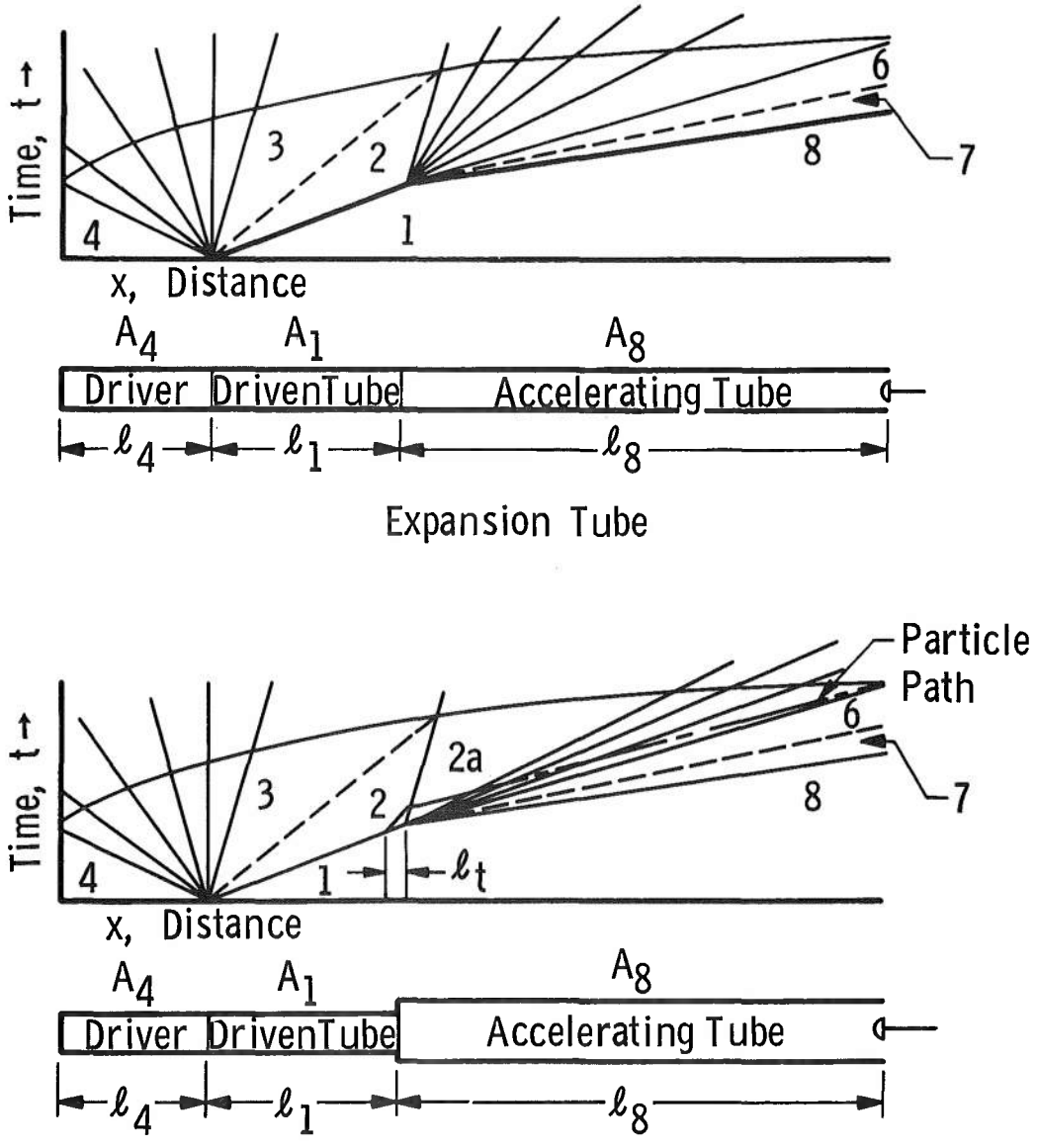

Fig. 3 Wave Diagram – Schematic

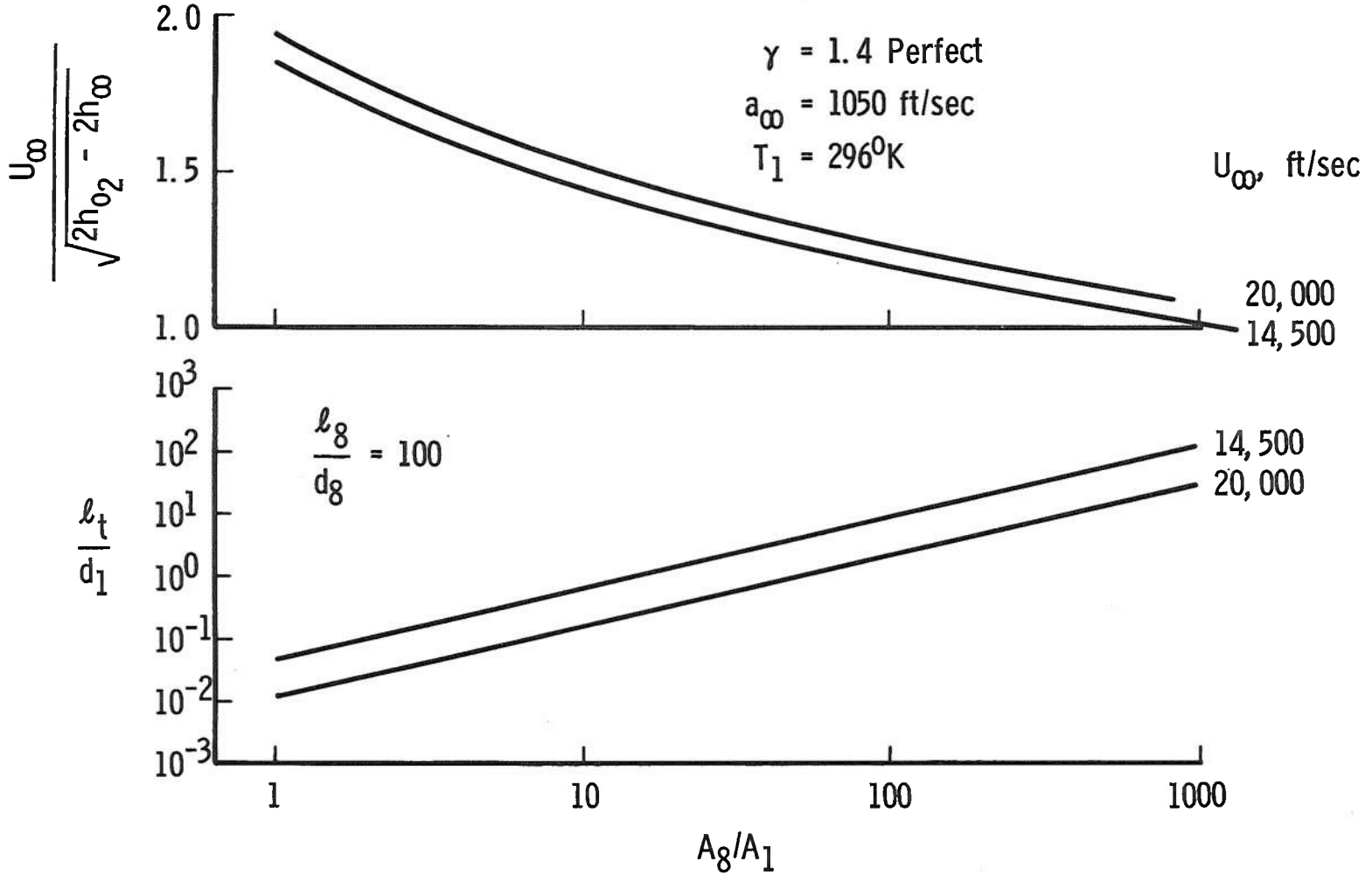

Fig. 4 Variation of Performance and Test Slug Length with Area Ratio

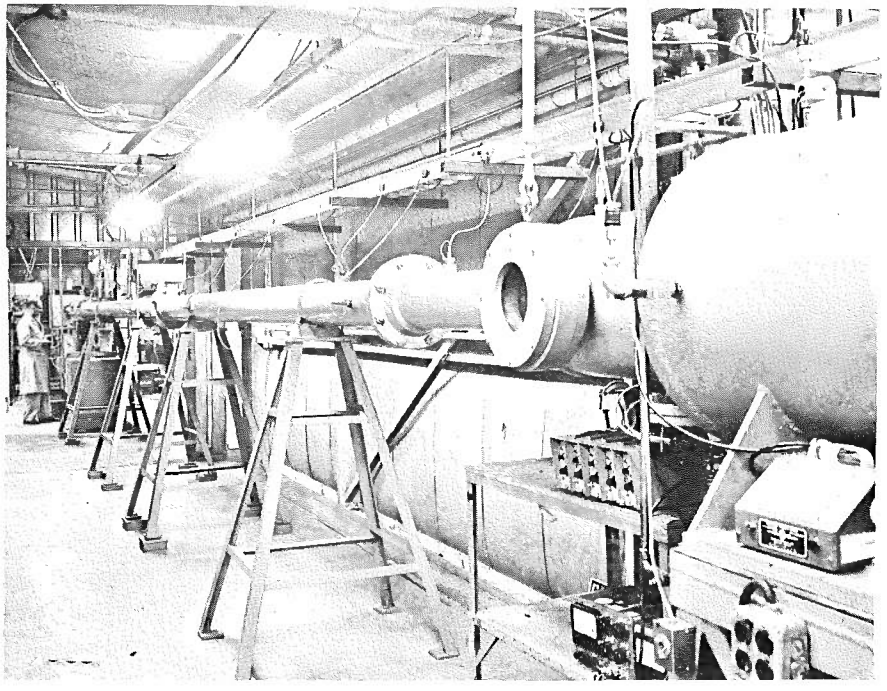

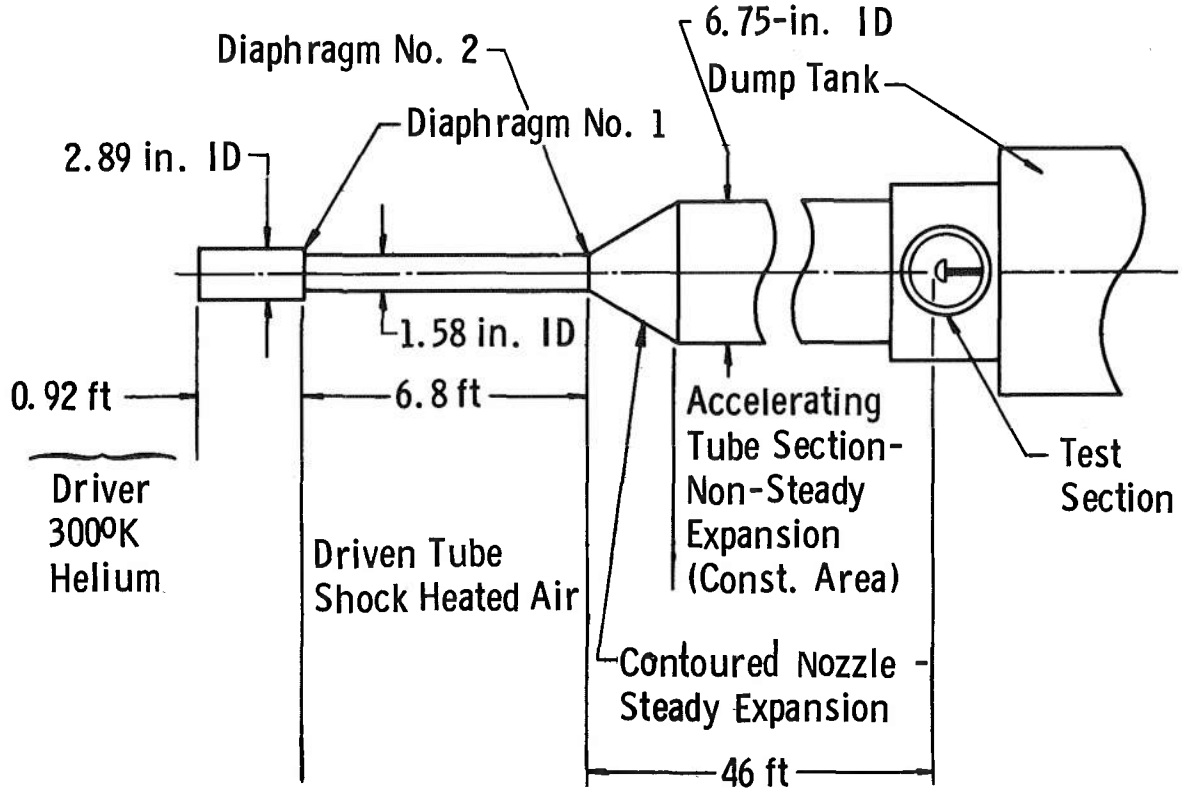

Fig. 5 AEDC-VKF Modified Expansion Tube

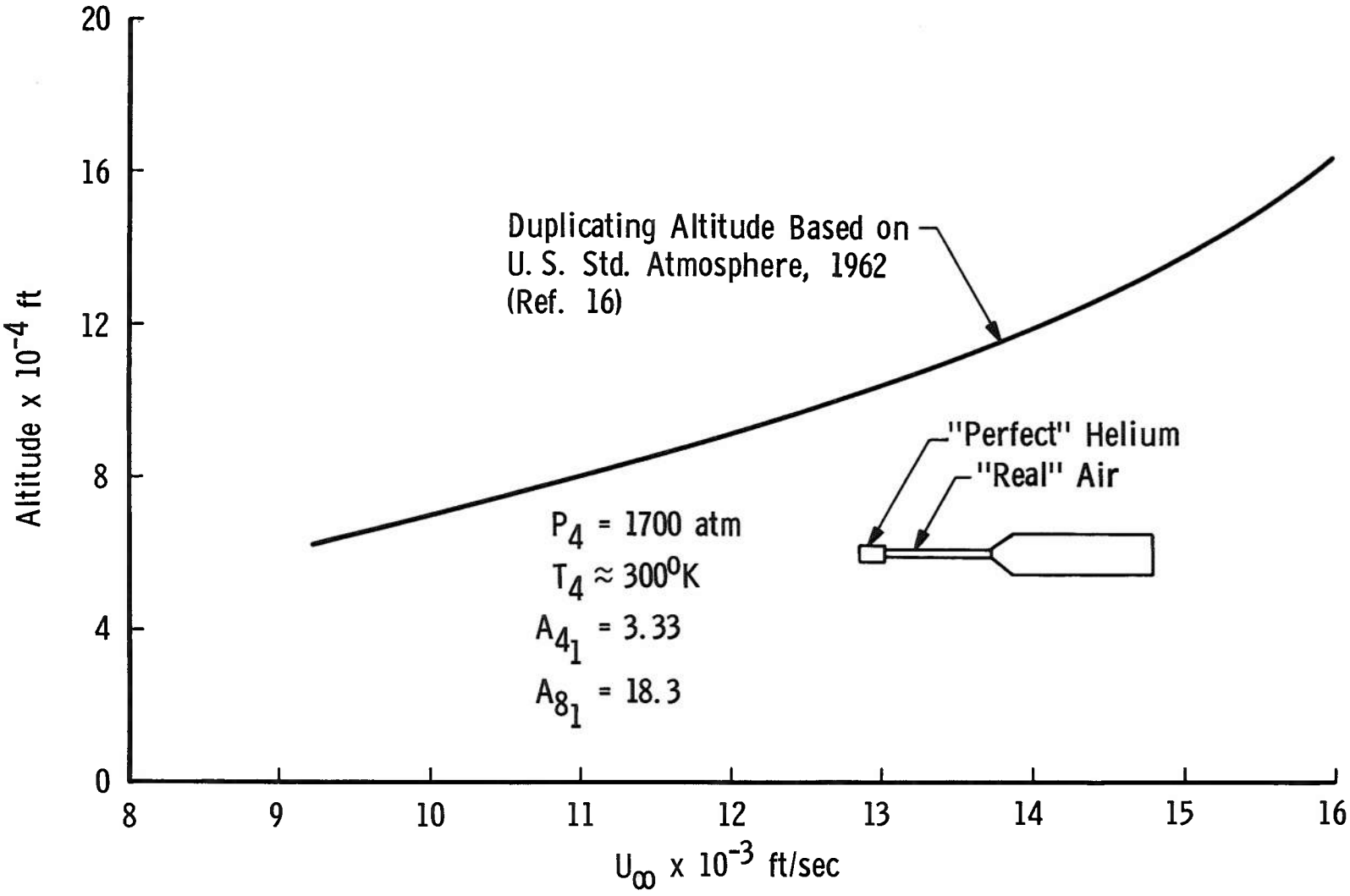

Fig. 6 Altitude-Velocity Regime, Modified Expansion Tube

	4	2	1	2a	6*	7	8
U, fps	0	6570	0	9300	14,100	14,100	0
P, atm	1700	28.7	0.55	0.44	3.61×10^{-3}	3.61×10^{-3}	14.5×10^{-6}
a, fps	3310	3070	1135	1960	1031	4350	1135
T, ^{o}K	290	2400	296	935	246	4350	296
M	0	2.12	0	4.75	13.7	3.25	0

* Duplicated Altitude ≈ 125,000 ft

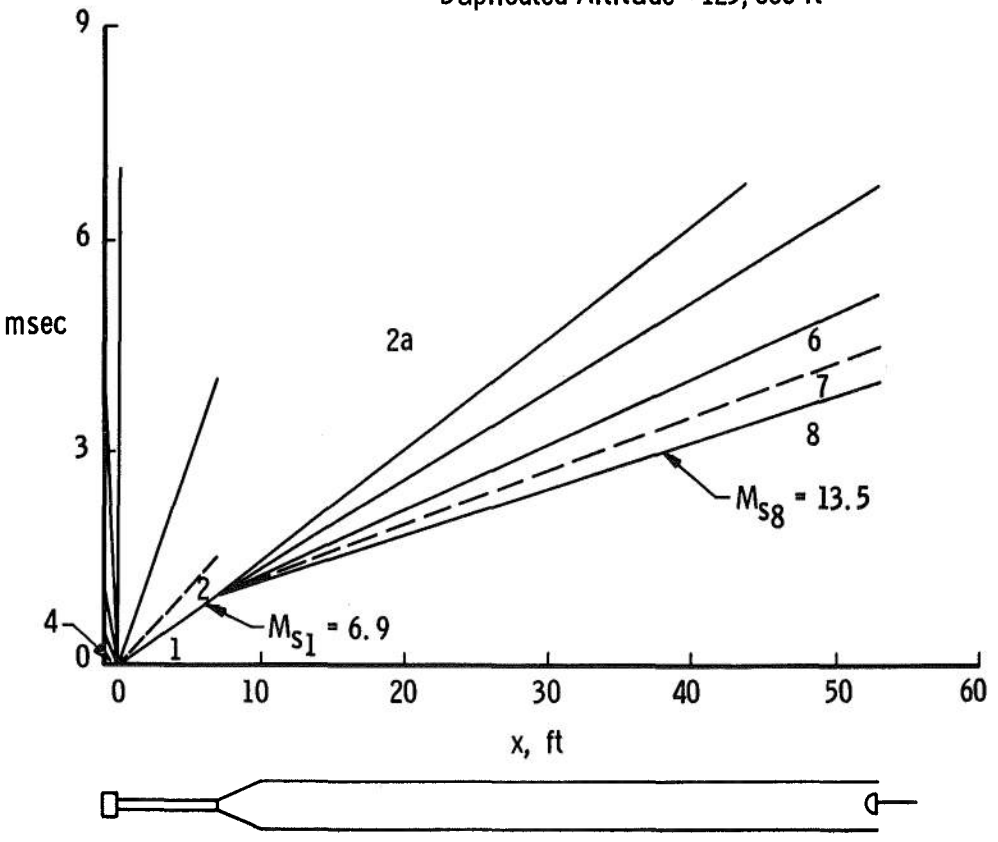

Fig. 7 Modified Expansion Tube – Flow Properties, "Standard Conditions"

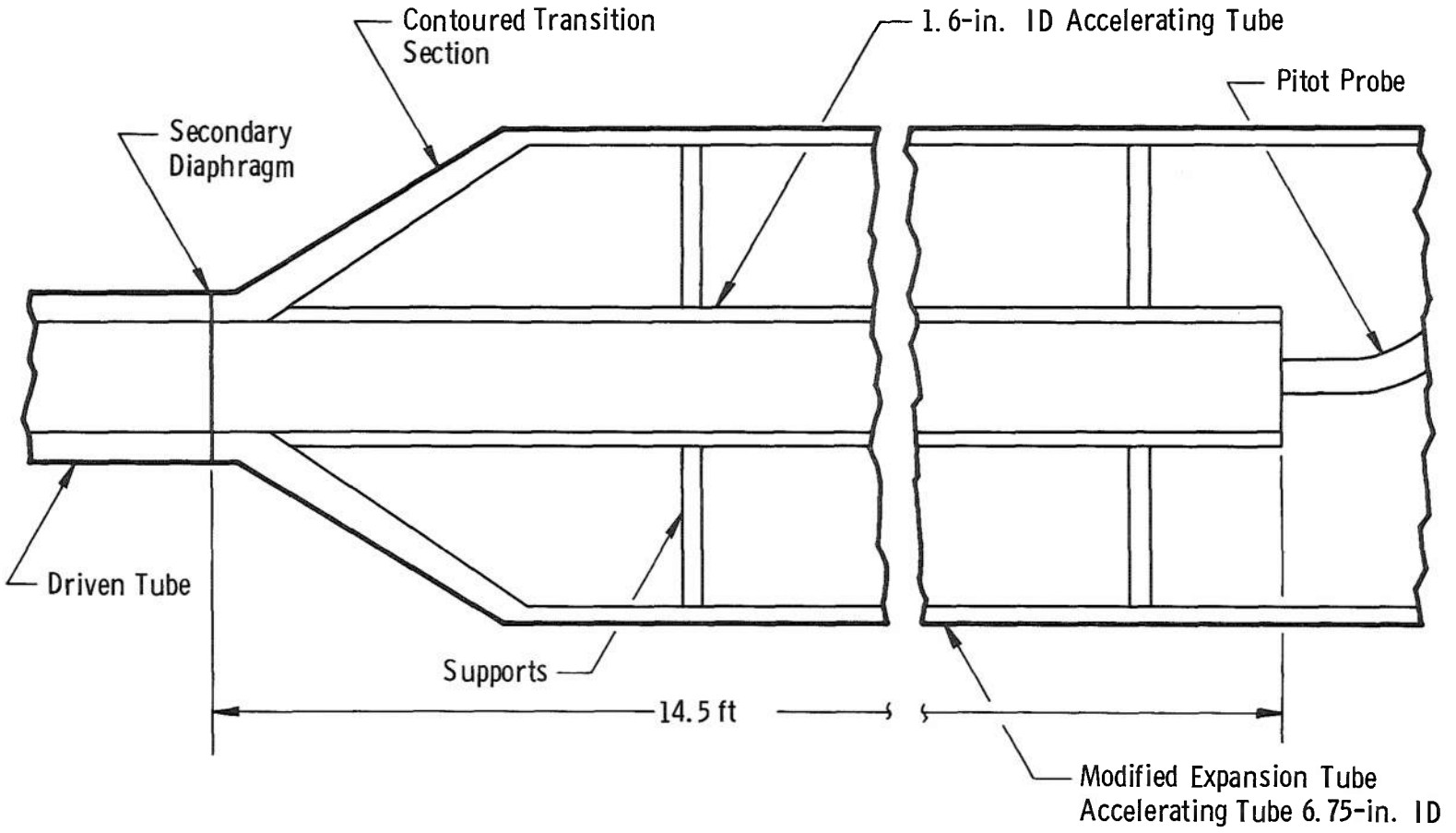

Fig. 8 Constant Area Tube Installation – Schematic

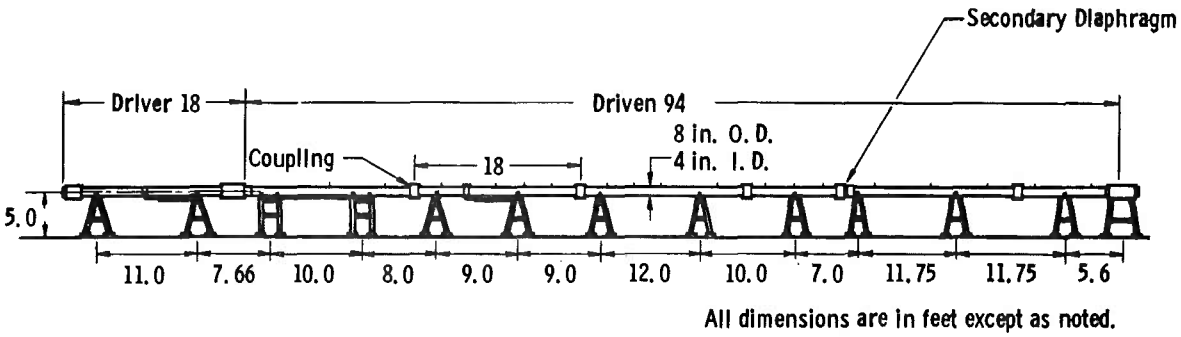

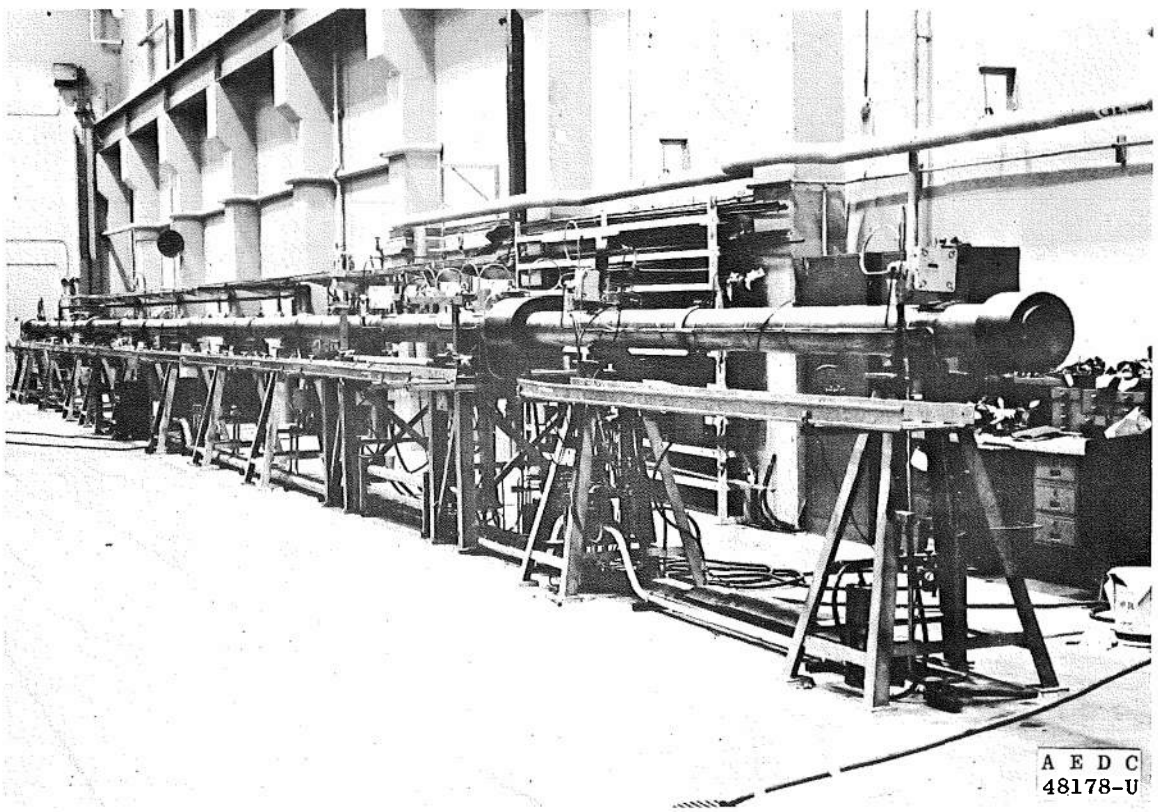

Fig. 9 AEDC-VKF High Density Shock Tube

	4	3	2	1	6	7	8
U, fps	0	5200	5200	0	16,500	16,500	0
P, atm	680	12.2	12.2	0.33	0.00673	0.00673	0.000021
a, fps	3350	1510	2830	1130	962	4800	1130
T, ^{o}K	296	59	1950	296	225	4920	296
M	0	3.44	1.84	0	17.20	3.44	0

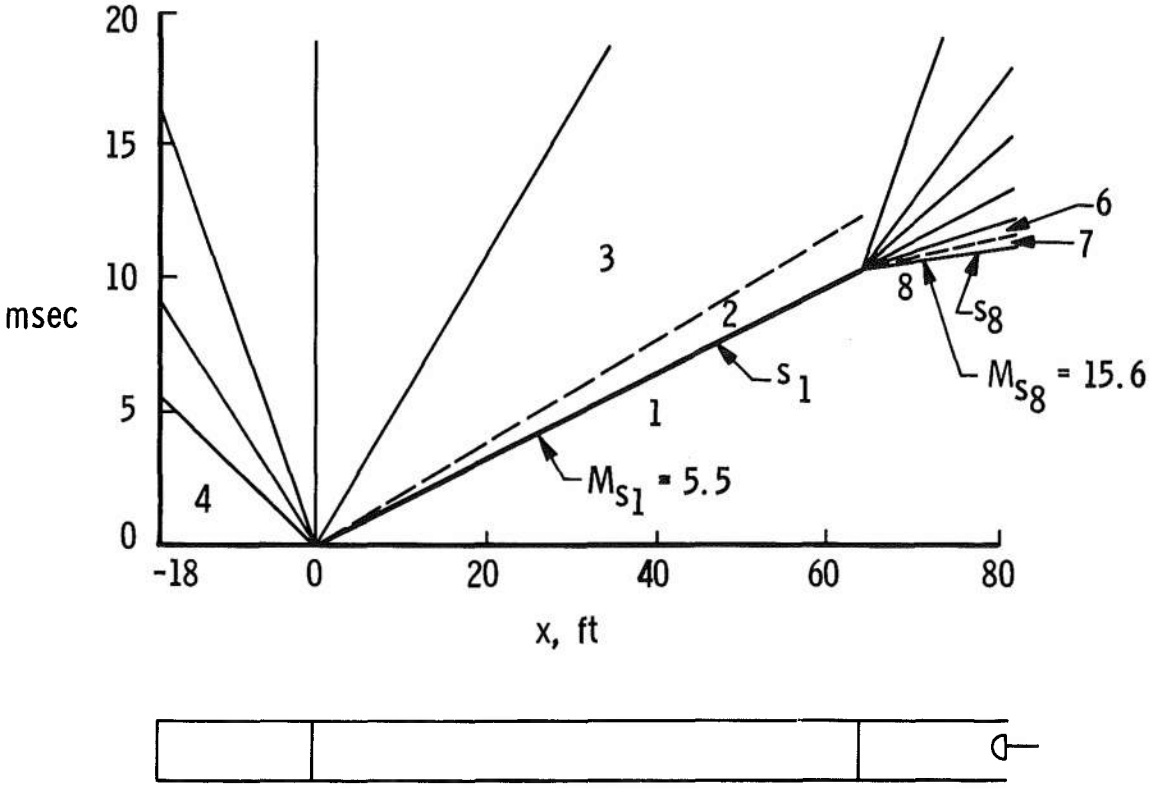

Fig. 10 High Density Shock Tube – Flow Properties (P_8 = 16 μHg)

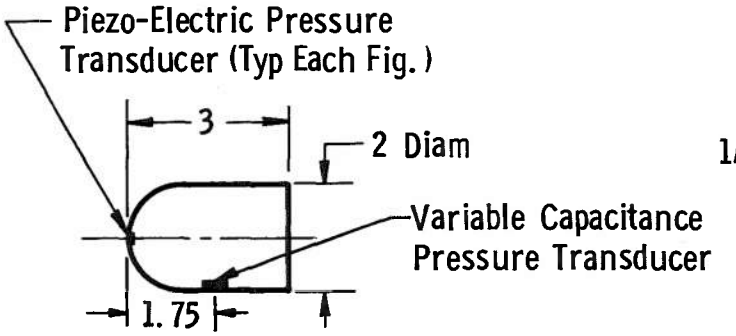

a. Hemisphere-Cylinder

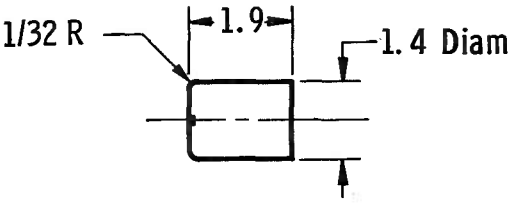

b. Flat-Faced Cylinder

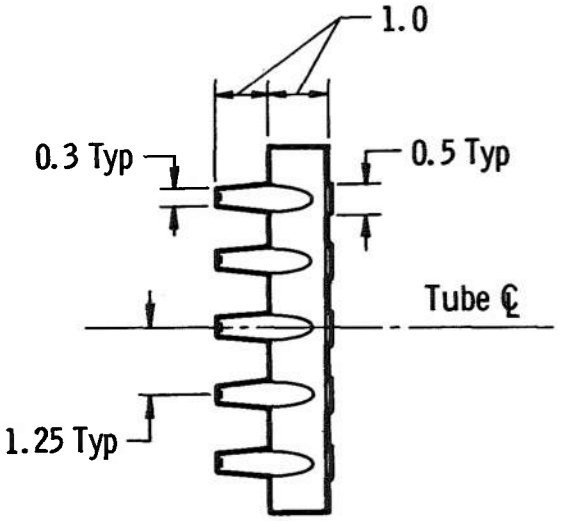

c. Pitot Rake

All Dimensions
in Inches

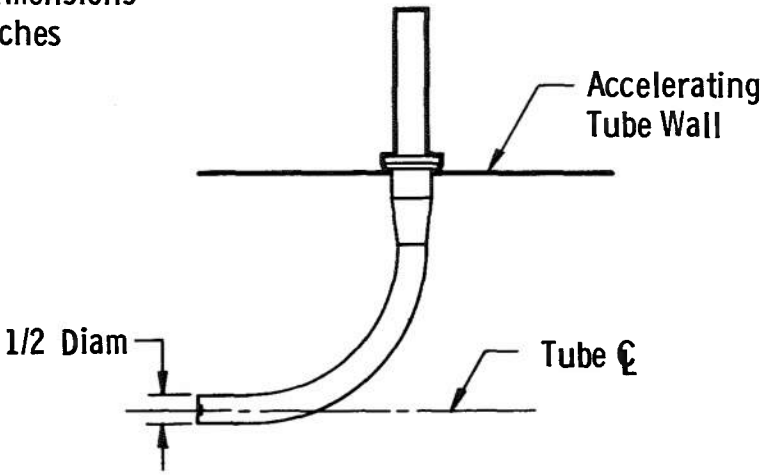

d. Pitot Probe

Fig. 11 Models – Modified Expansion Tube

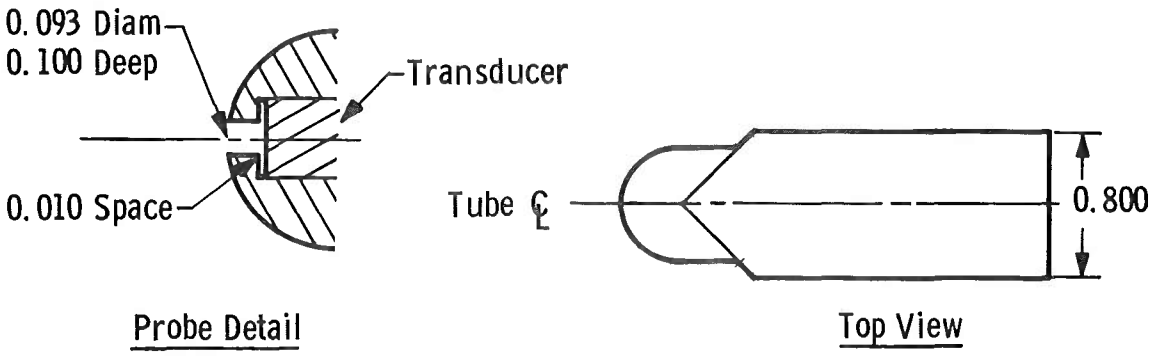

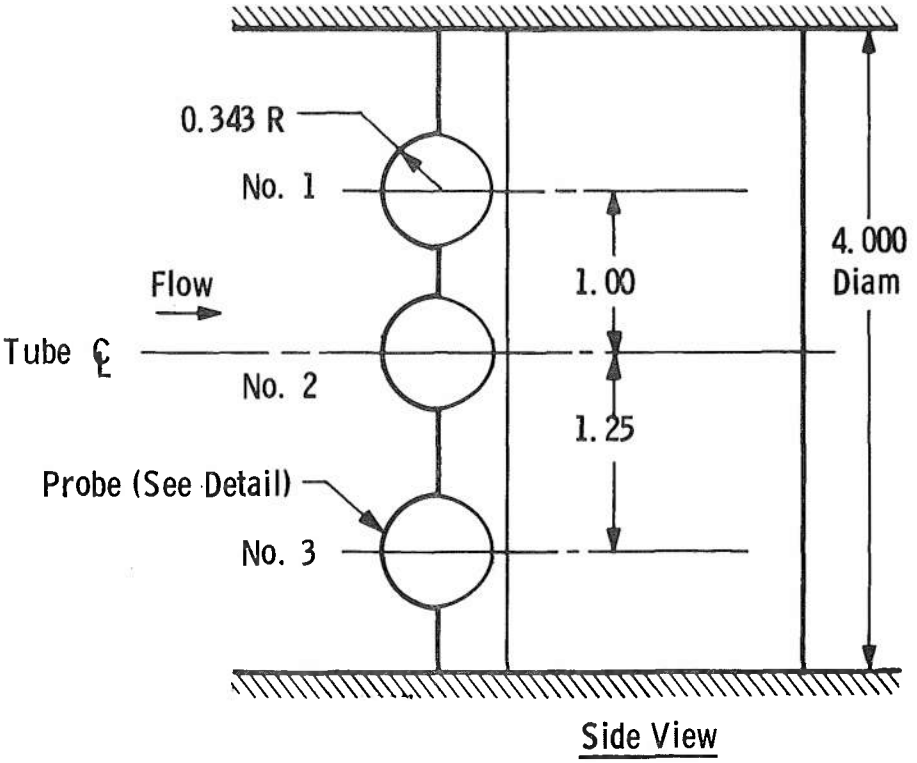

Note: All Dimensions in Inches

Fig. 12 Pitot Rake – High Density Shock Tube

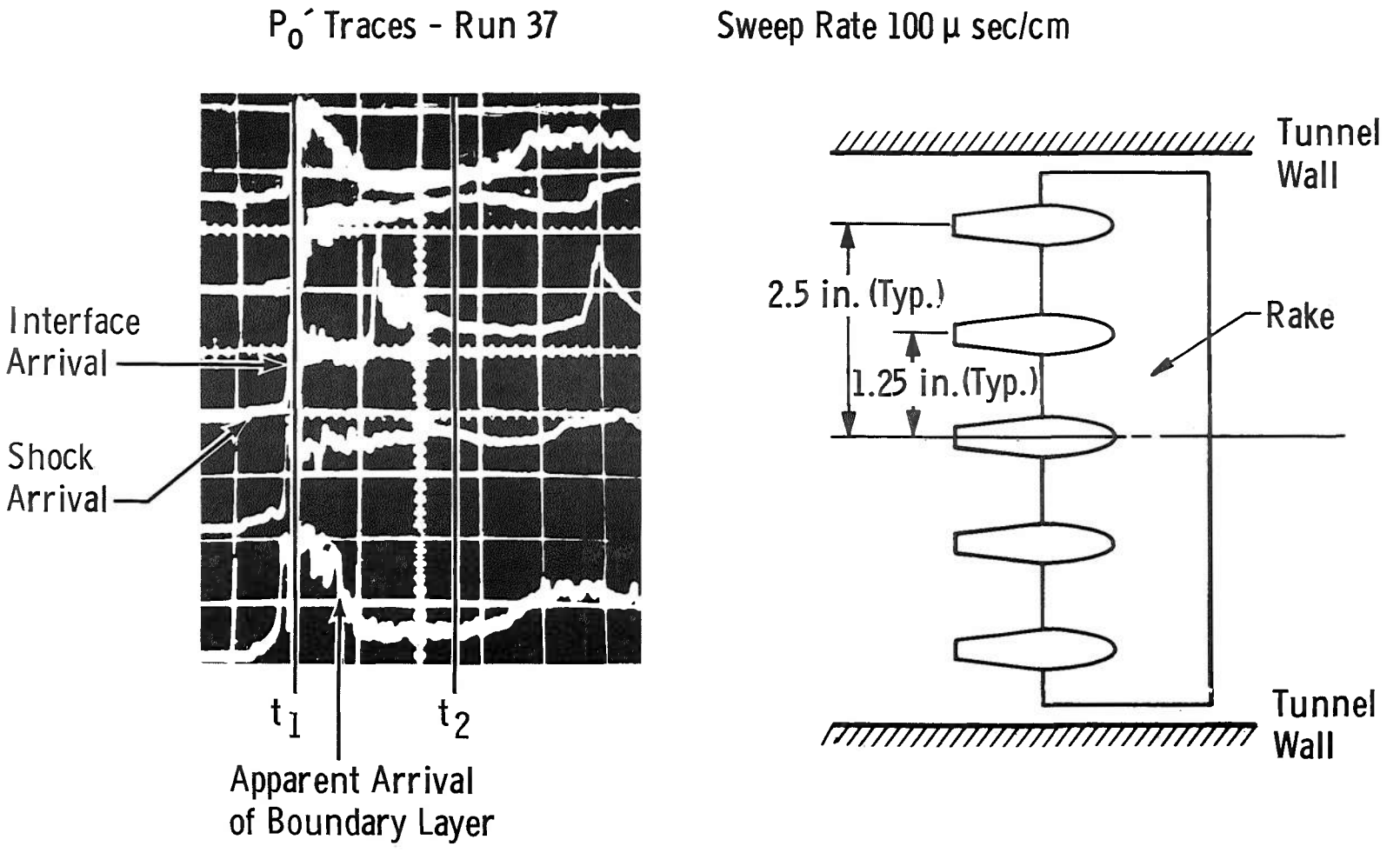

Fig. 13 Sketch of Rake and Sample Pitot Pressure – 6.75-in. Modified Expansion Tube

Run 21

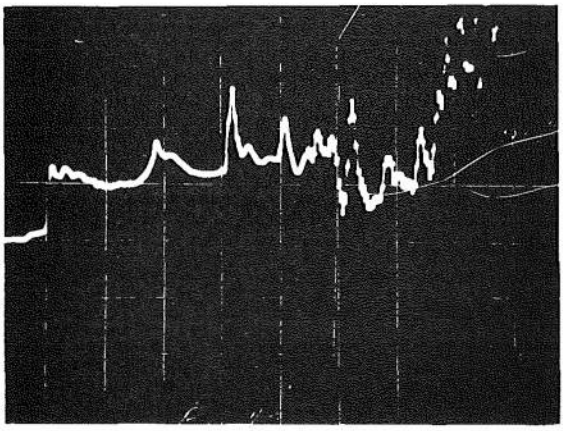

P_4 - 462 to 490 atm (Helium)

P_1 - 304 mm Hg (Air)

P_8 - 18 μ Hg (Air)

M_{s_8} - 10.8 to 11.4

ℓ_8 - 46 ft

Sweep Rate - 200 μ sec/cm

Run 23

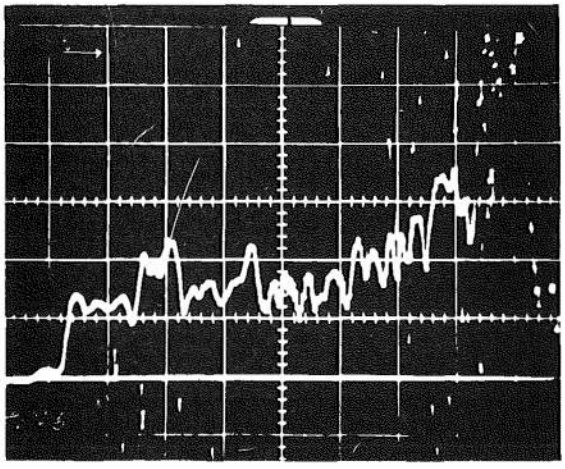

Run 25

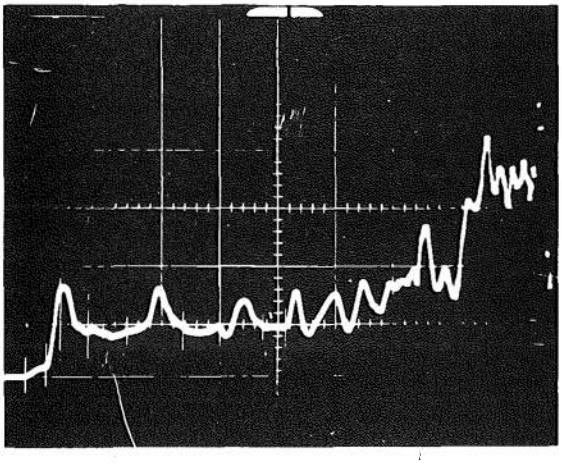

Fig. 14 Typical Pitot Traces for a Flat Face Cylinder Model

P_4 - 1190 to 1260 atm (Helium)

P_1 - 455 mm Hg (Air)

P_8 - 17 μ Hg (Air)

ℓ_8 - 46 ft

M_{s8} - 13.7 to 13.3

Sweep Rate 100 μ sec/cm

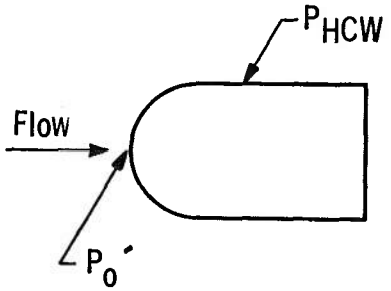

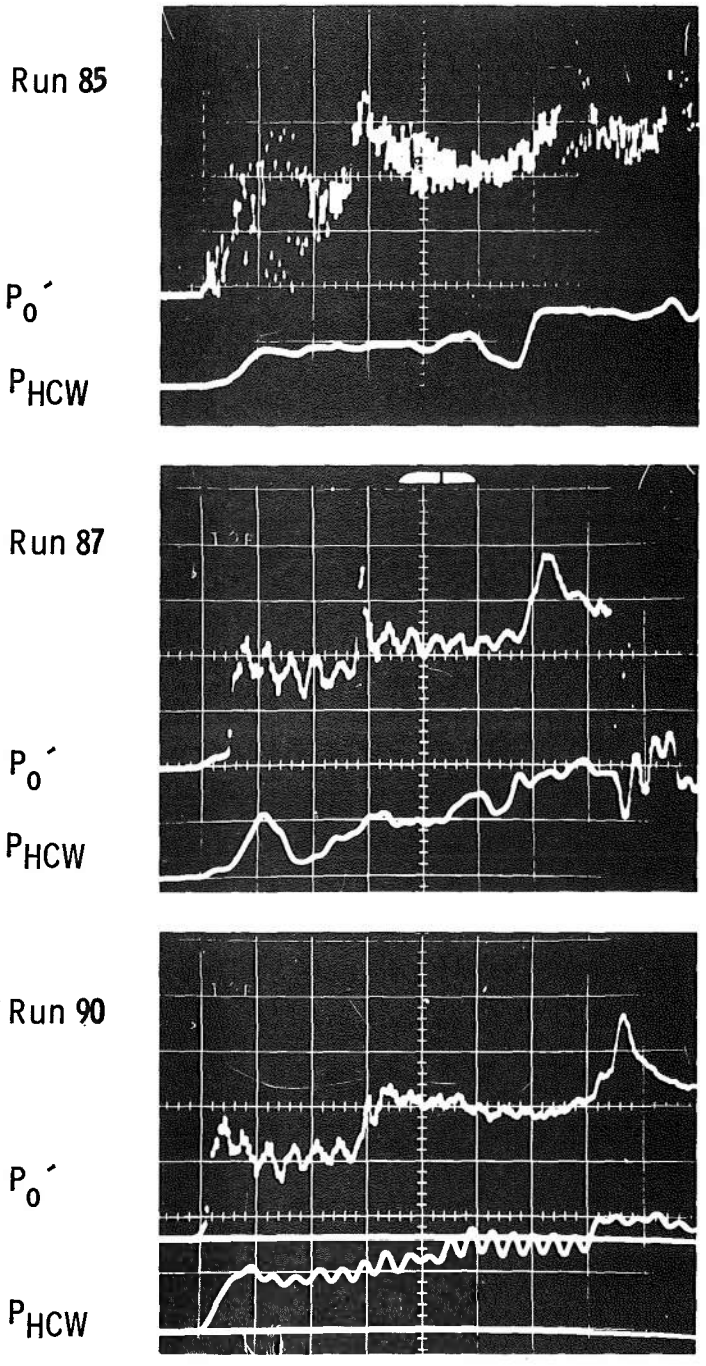

Fig. 15 Typical Pitot Traces for a Hemisphere-Cylinder Model

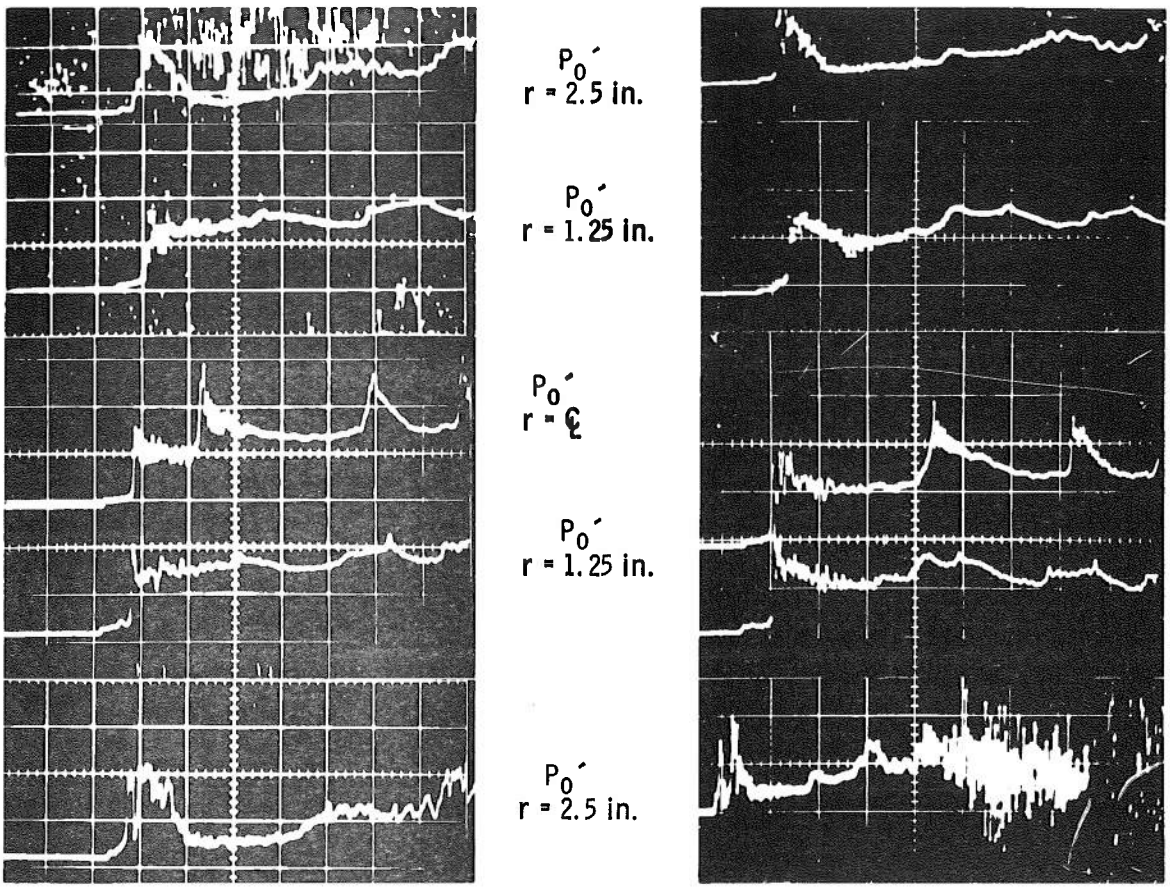

Run 37
ℓ_8 = 38.5 ft

Run 41
ℓ_8 = 42 ft

P_4 - 455 atm
P_1 - 304 mm Hg (Air)
P_8 - 18 μ Hg (Air)
M_{s_8} 10.9 to 11.8
Sweep Rate 100 μ sec/cm
Note: Sweep Rate Run 41 P_0' (r = 2.5 in.) 200 μ sec/cm

Fig. 16 Pitot Rake Traces – Two Different Accelerating Tube Lengths

P_4 - 440 to 483 atm (Helium)

P_1 - 320 mm Hg (Air)

P_8 - 18 μ Hg (Air)

M_{s_8} - 11.5 to 7100

Sweep Rate - 100 μ sec/cm

Run 47
ℓ_8 = 46

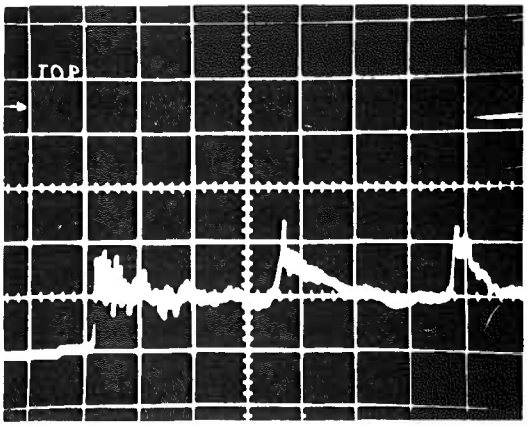

Run 48
ℓ_8 = 27.44

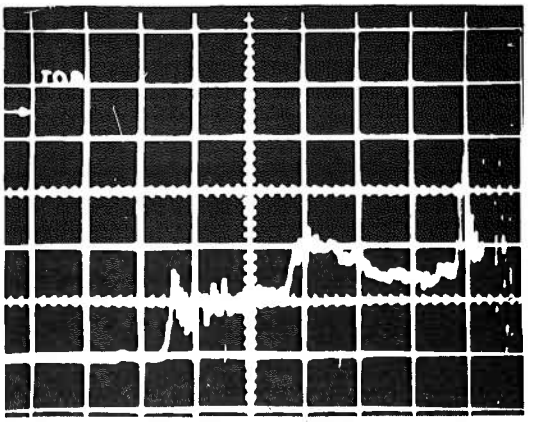

Run 49
ℓ_8 = 17

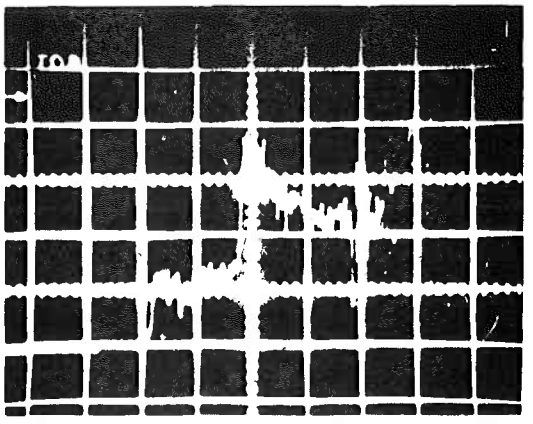

Fig. 17 Typical Traces for a Centerline Pitot Probe

Run 99

P_4 - 1210 atm - Helium
P_1 - 310 mm Hg - Air
P_8 - 60 μ Hg 16% Air 84% Helium
Sweep Rate - 100 μ sec/cm
Vert. Sens. P_0' - 100 mv/cm

Note: Percent Composition by Volume

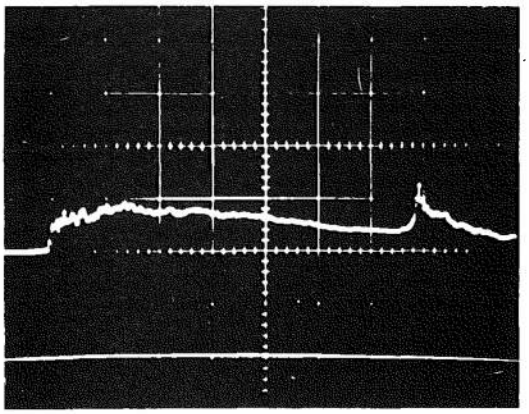

Run 105

P_4 - 1520 atm - Helium
P_1 - 452 mm Hg - Air
P_8 - 40 μ Hg 25% Air 75% Helium
Sweep Rate - 200 μ sec/cm
Vert. Sens. P_0' - 50 mv/cm

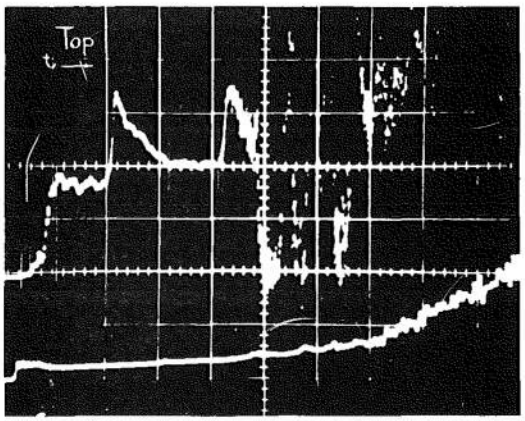

Run 107

P_4 - 1480 atm - Helium
P_1 - 452 mm Hg - Air
P_8 - 100 μ Hg 10% Air 90% Helium
Sweep Rate - 200 μ sec/cm
Vert. Sens. P_0' - 50 mv/cm

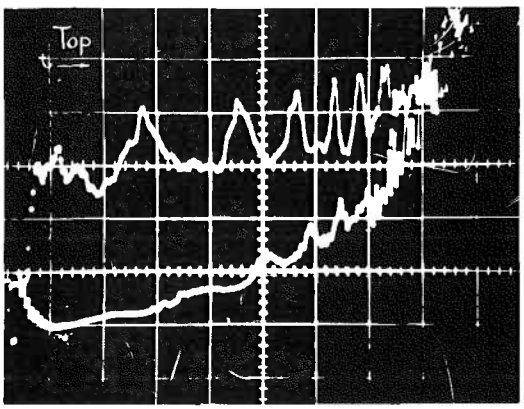

Fig. 18 Typical Pitot Traces for Helium-Air Mixture Accelerating Gas (Hemisphere-Cylinder Model)

Hemisphere - Cylinder

ℓ_8 = 46 ft

$M_{s_1} \approx 7.0$

P_1 = 452 mm Hg

$M_{s_8} \approx 13.8$

P_8 = 18 μ Hg

(Scope Triggered by Shock Approximately 3.7 ft Upstream of Model, Sweep Rate 200 μ sec/cm)

$\tau_7 \approx 183$ μ sec

$\tau_6 \approx 220$ μ sec

Run 152

P_0

P_6

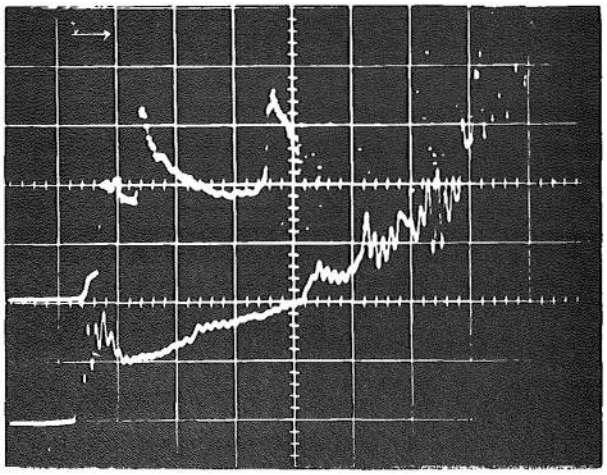

Run 157

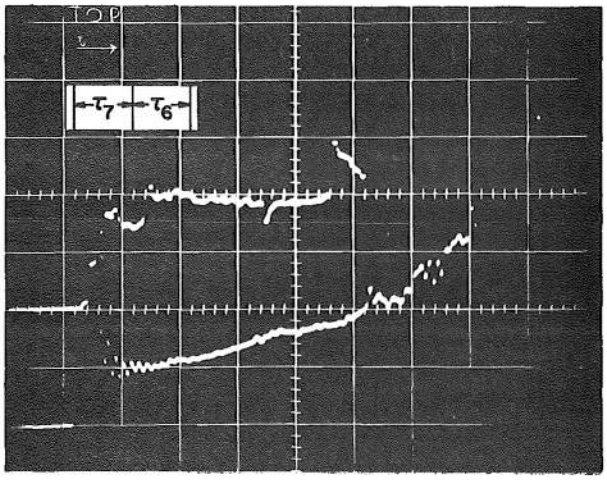

Run 161

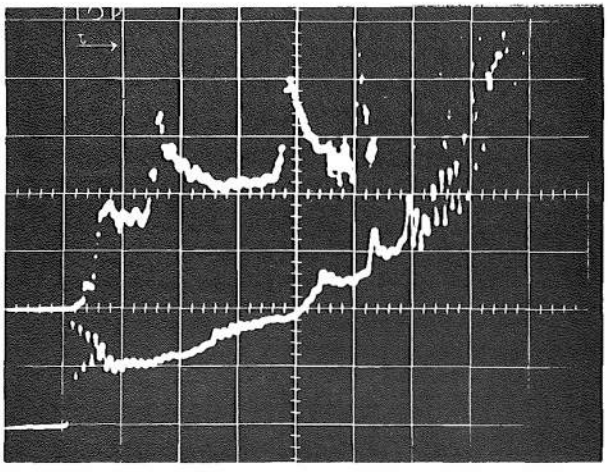

Fig. 19 Pitot and Static Pressure Traces, d_8 = 6.75 in., One 3/4-mil Polyester

Hemisphere - Cylinder

ℓ_8 = 46 ft

$M_{s_1} \approx 7.0$

P_1 = 452 mm Hg

$M_{s_8} \approx 13.8$

P_8 = 18 μ Hg

(Scope Triggered by Shock Approximately 3.7 ft Upstream of Model, Sweep Rate 200 μ sec/cm)

$\tau_7 \approx 183$ μ sec

$\tau_6 \approx 220$ μ sec

Run 151

P_0

P_6

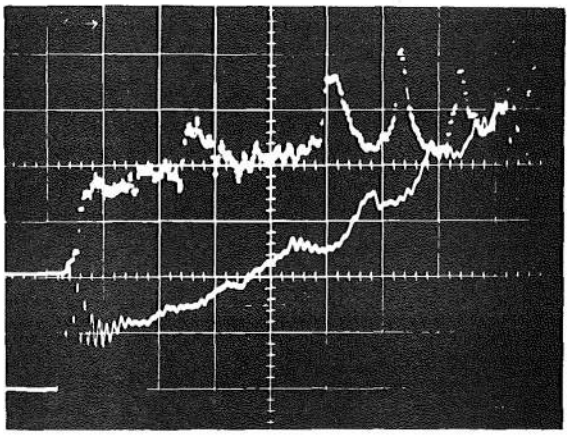

Run 155

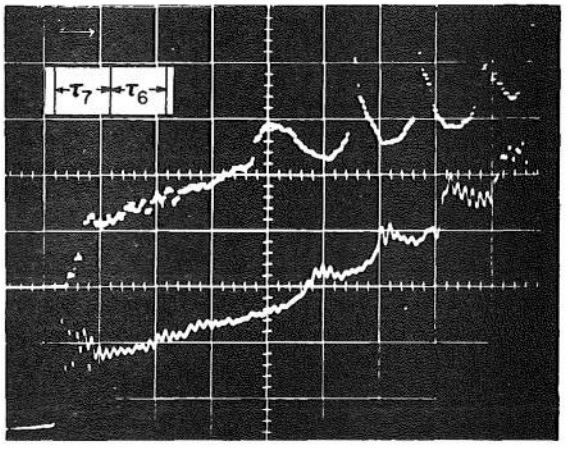

Run 156

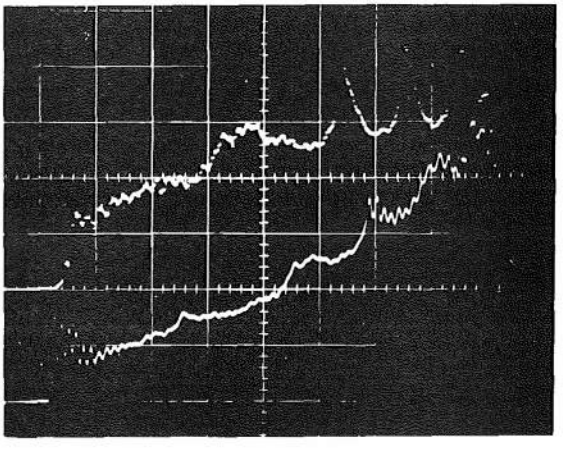

Fig. 20 Pitot and Static Pressure Traces, d_8 = 6.75 in., One 3/4-mil Aluminum Foil

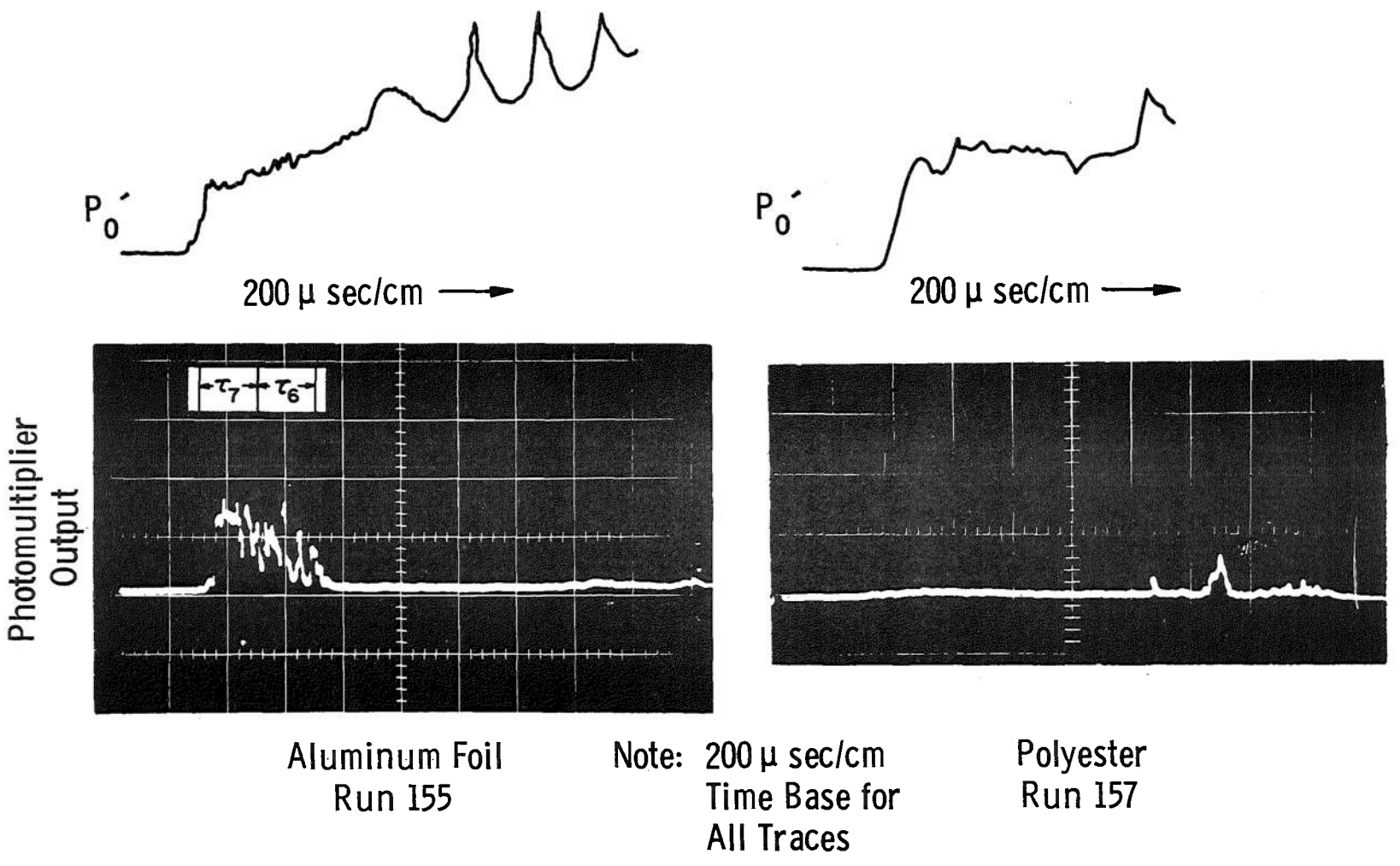

Fig. 21 Monochromatic (≈3090 Å) Radiation Using Aluminum Foil and Polyester Secondary Diaphragm

Run 180

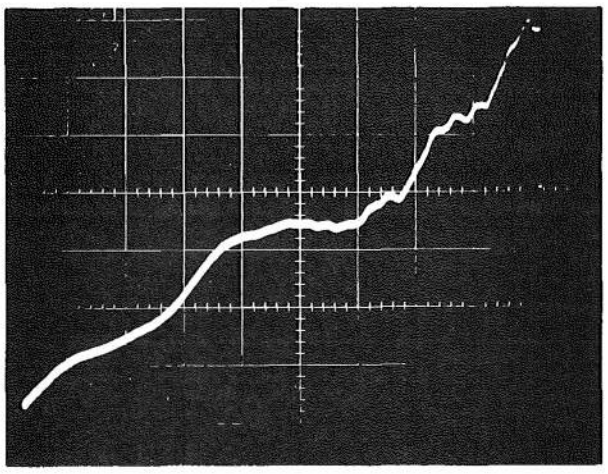

ℓ_8 = 14.5 ft

$M_{s_1} \approx 7.4$

P_1 = 544 mm Hg (Air)

Run 182

$M_{s_8} \approx 18.0$

P_8 = 18 μ Hg (Air)

(Scope Triggered off Rise, Sweep Rate 20 μ sec/cm)

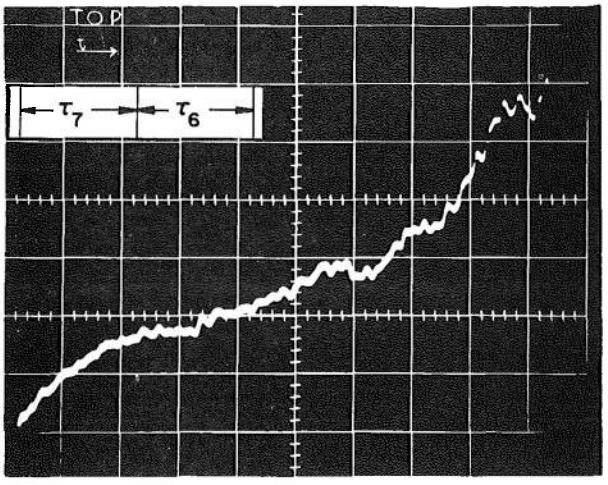

$\tau_7 \approx 42$ μsec

$\tau_6 \approx 40$ μsec

Run 185

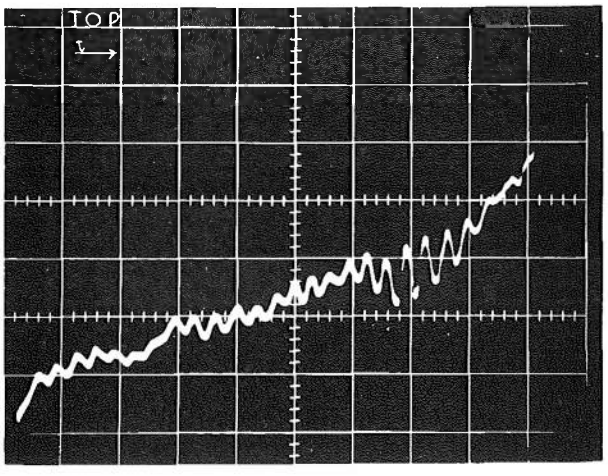

Fig. 22 Pitot Pressure Traces, d_8 = 1.60 in., One 3/4-mil Polyester

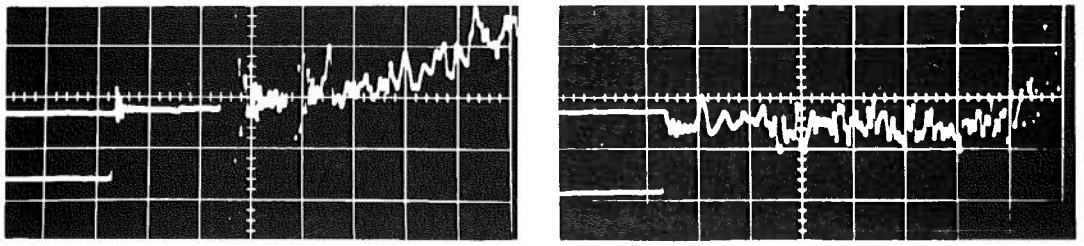

Run 156

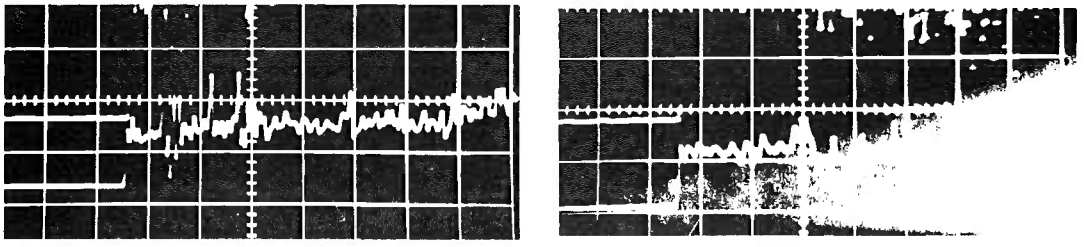

Run 158

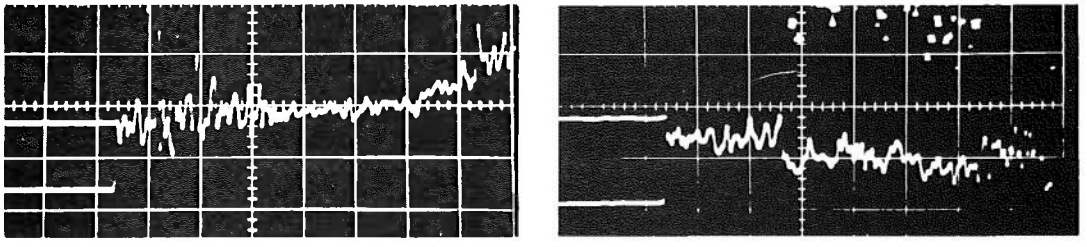

Run 159

$M_{S_1} \approx 5.5$

P_1 = 251 mm Hg

Sweep Rate 200 μ sec/cm

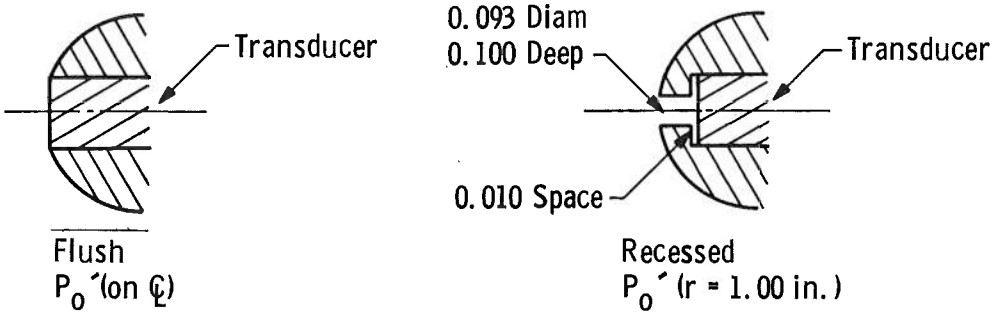

Probe Details

Fig. 23 Comparison of Flush and Recessed Mounting of Pressure Transducer

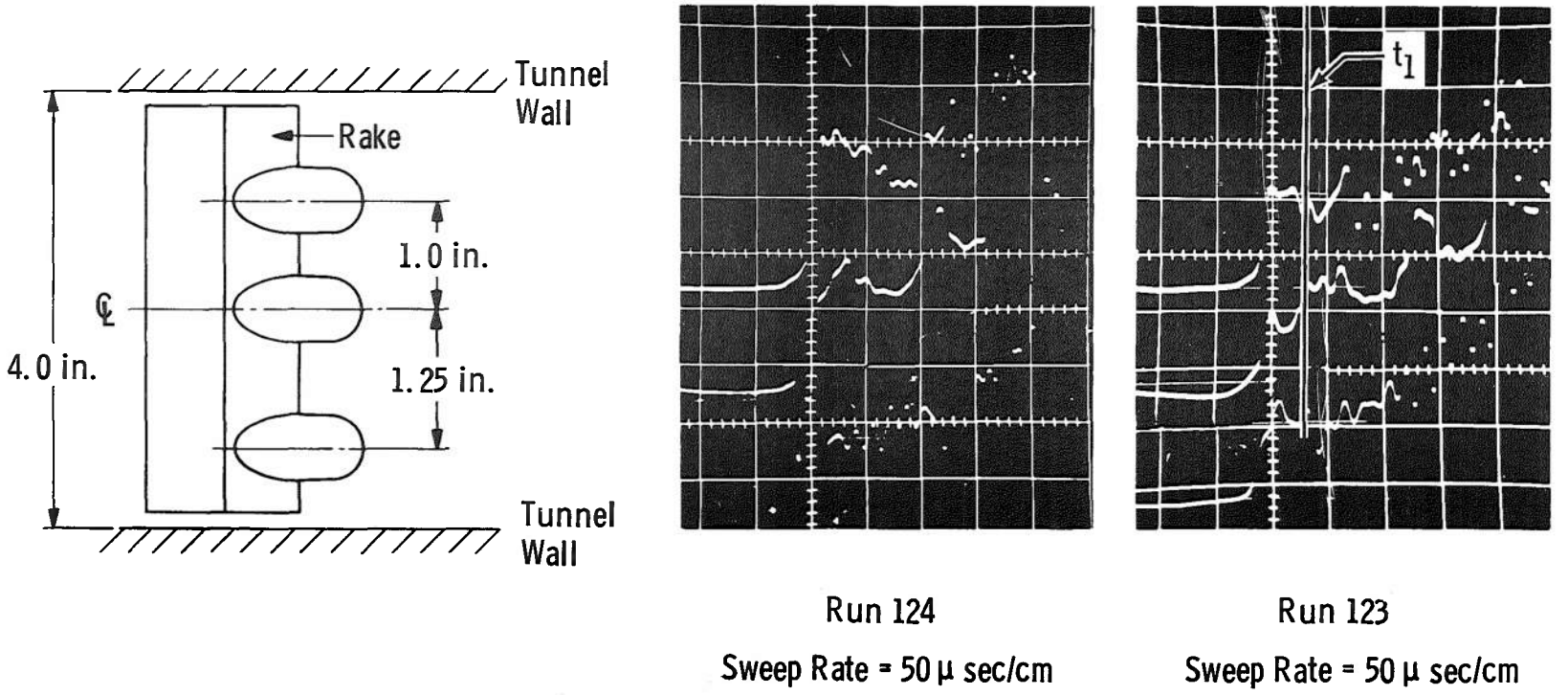

Fig. 24 Sketch of Rake and Sample Pitot Pressure Traces High Density Shock Tube, P_8 = 16 μHg

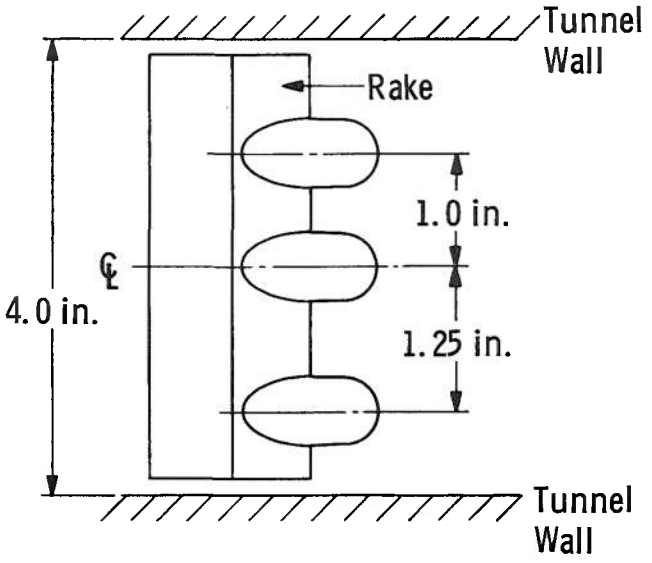

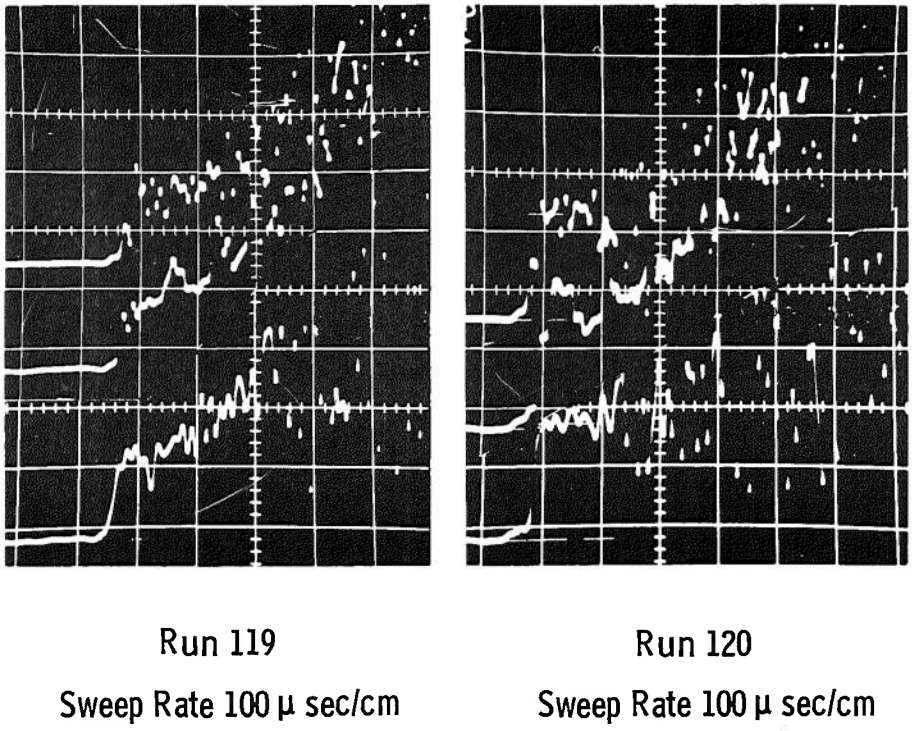

Run 119
Sweep Rate 100 μ sec/cm

Run 120
Sweep Rate 100 μ sec/cm

Fig. 25 Sketch of Rake and Sample Pitot Pressure Traces High Density Shock Tube, P_8 = 100 μHg

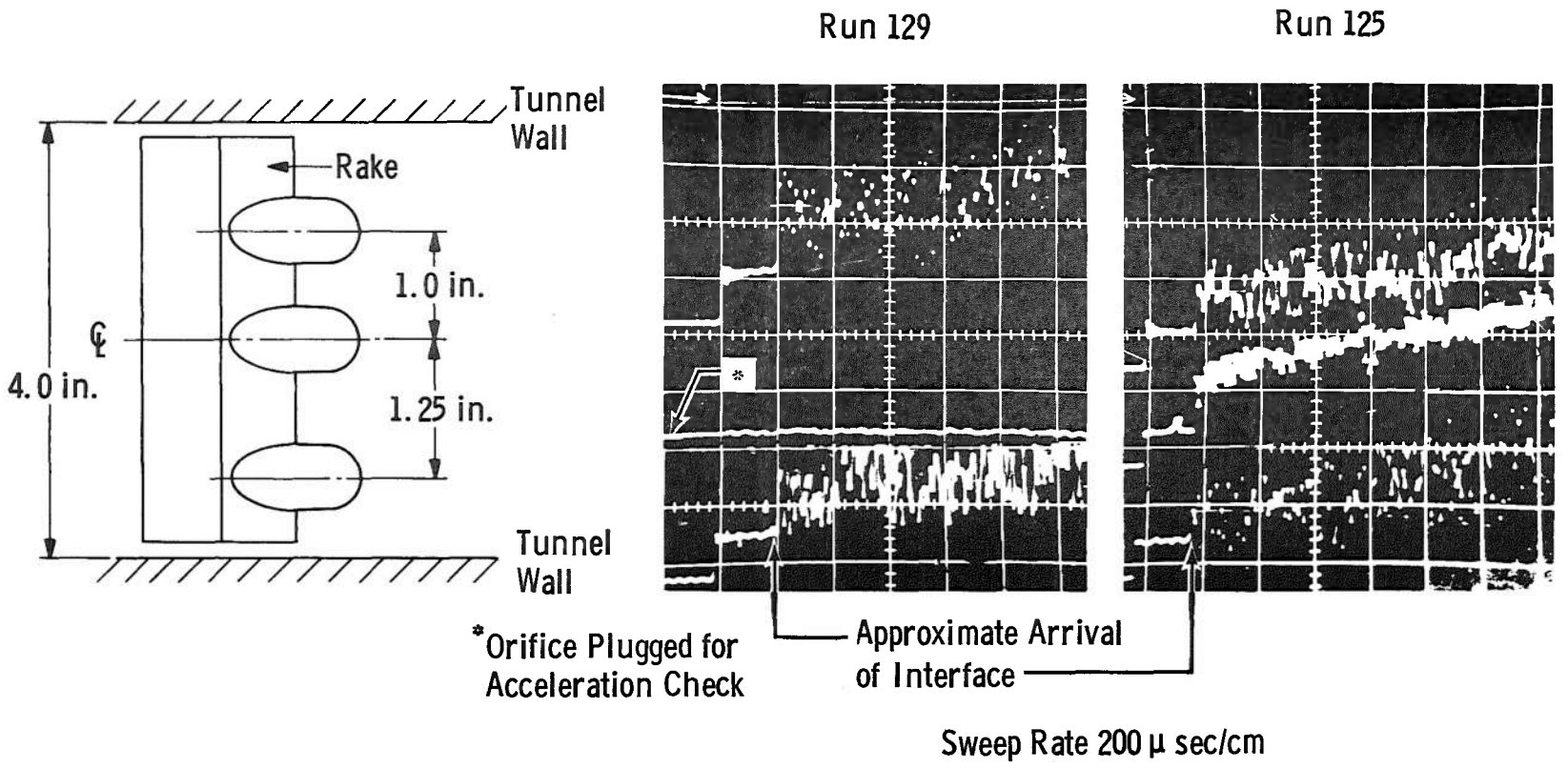

Fig. 26 Sketch of Rake and Sample Pitot Pressure Traces High Density Shock Tube, $P_8 = 18$ mm Hg

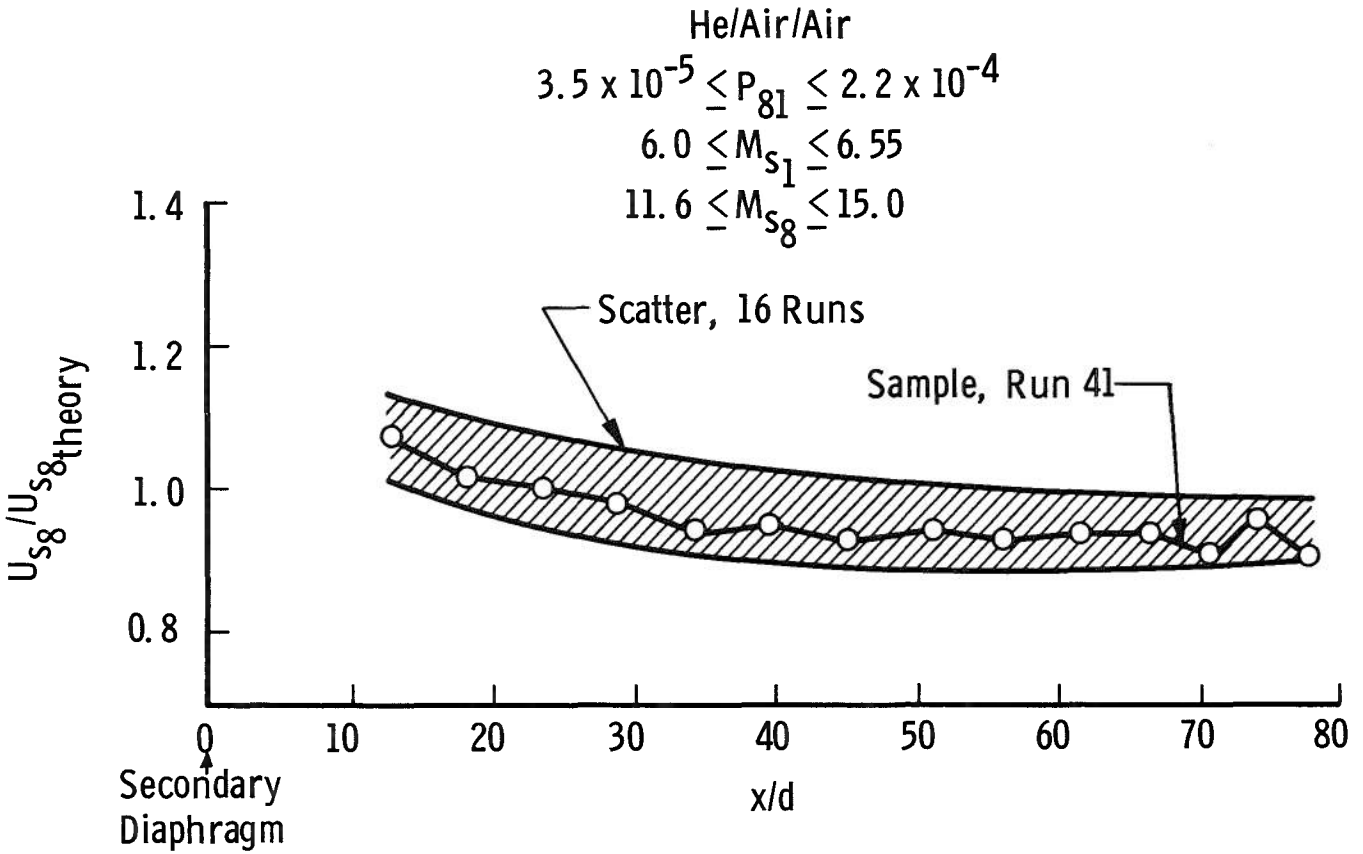

Fig. 27 Accelerating Tube Shock Velocity – Modified Expansion Tube

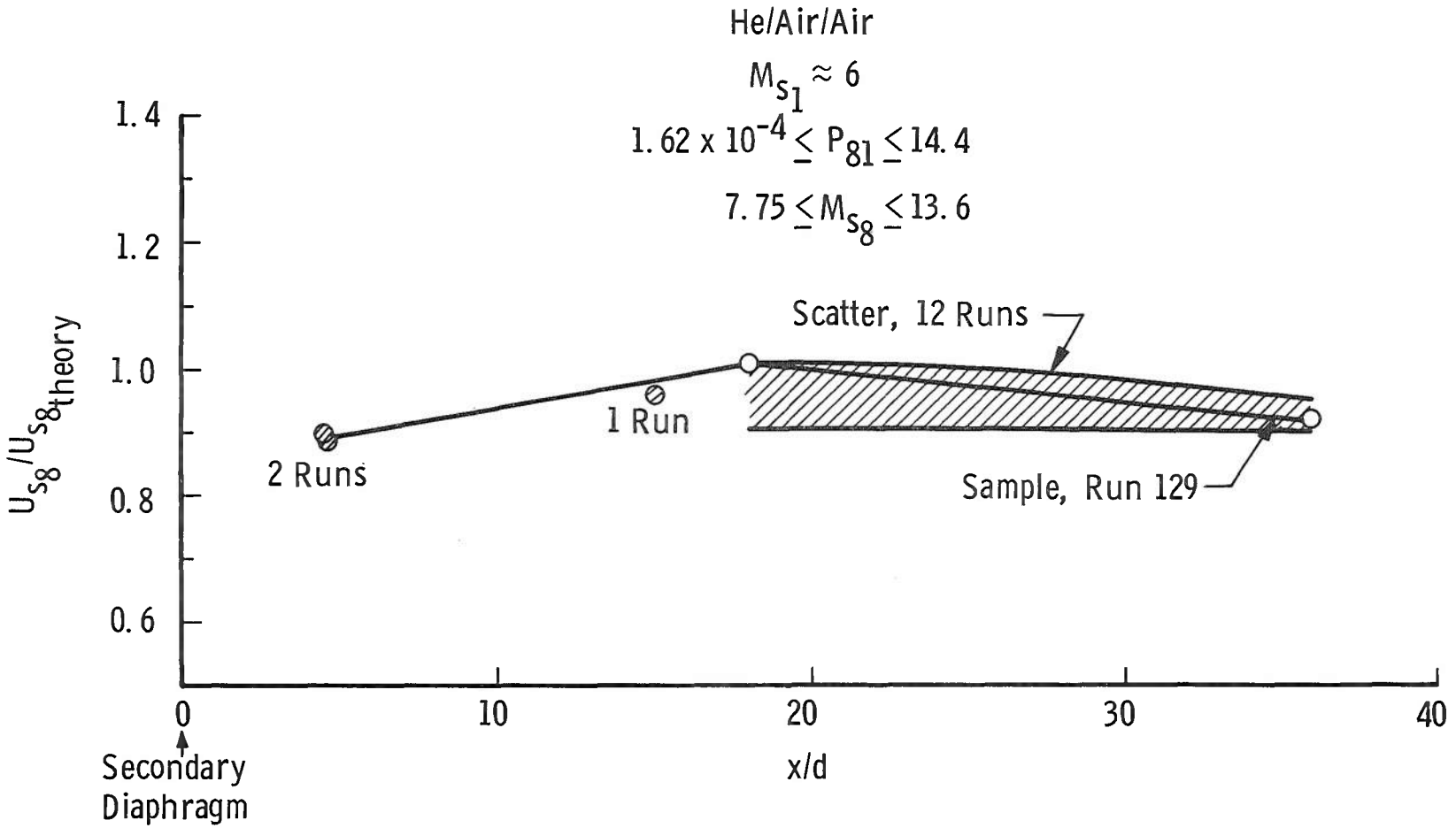

Fig. 28 Accelerating Tube Shock Velocity – High Density Shock Tube

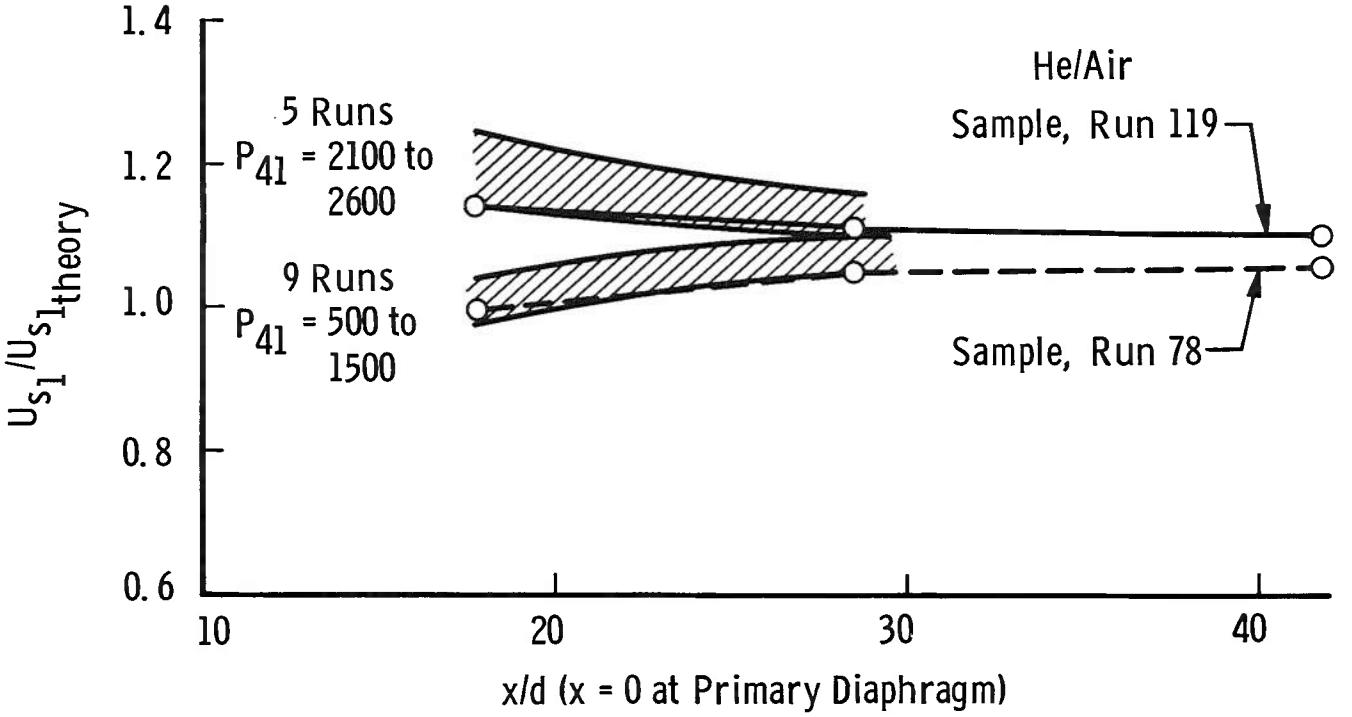

Fig. 29 Driven Tube Shock Velocity – Modified Expansion Tube

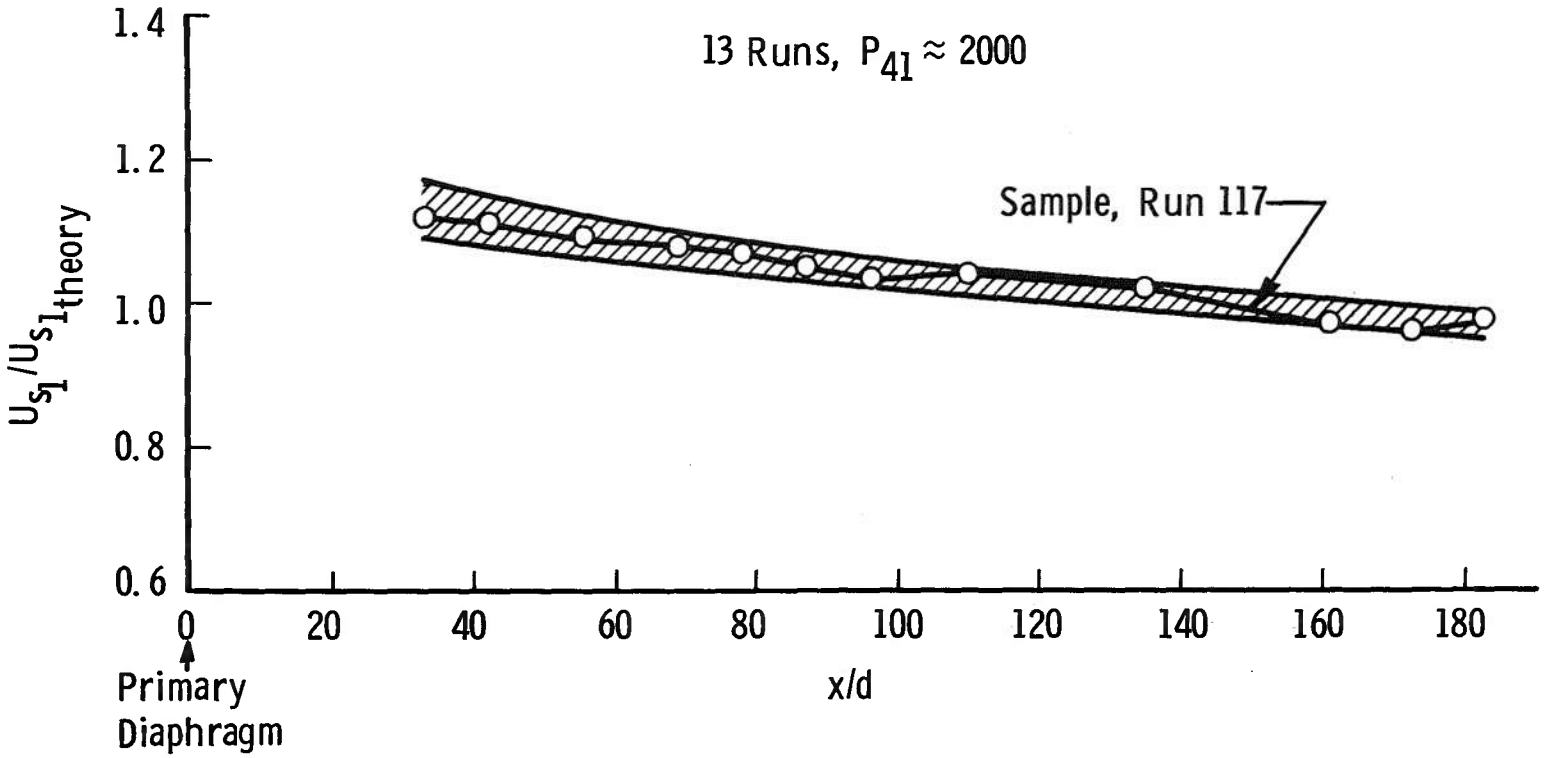

Fig. 30 Driven Tube Shock Velocity – High Density Shock Tube

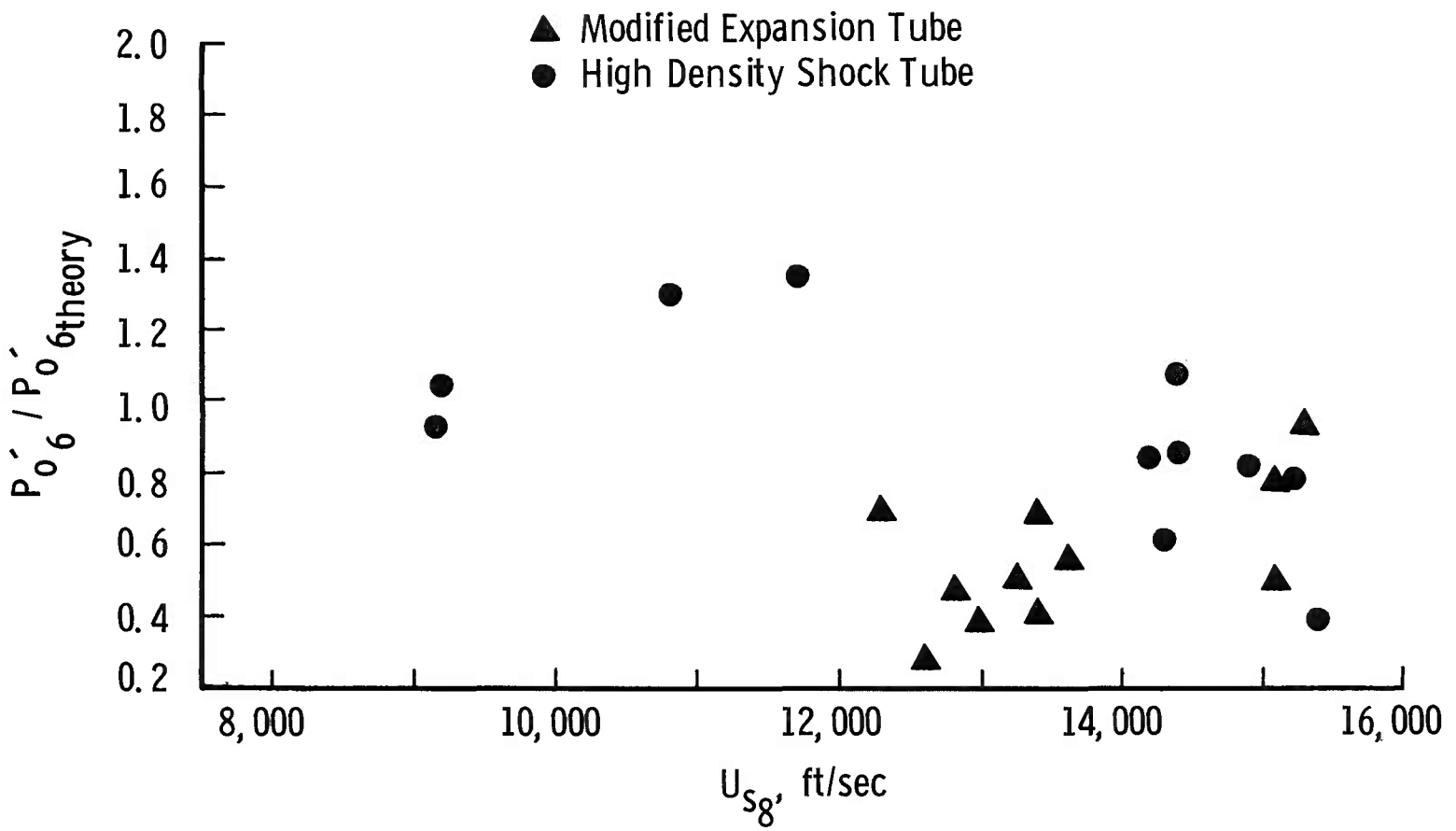

Fig. 31 Pitot Pressure at the Test Section

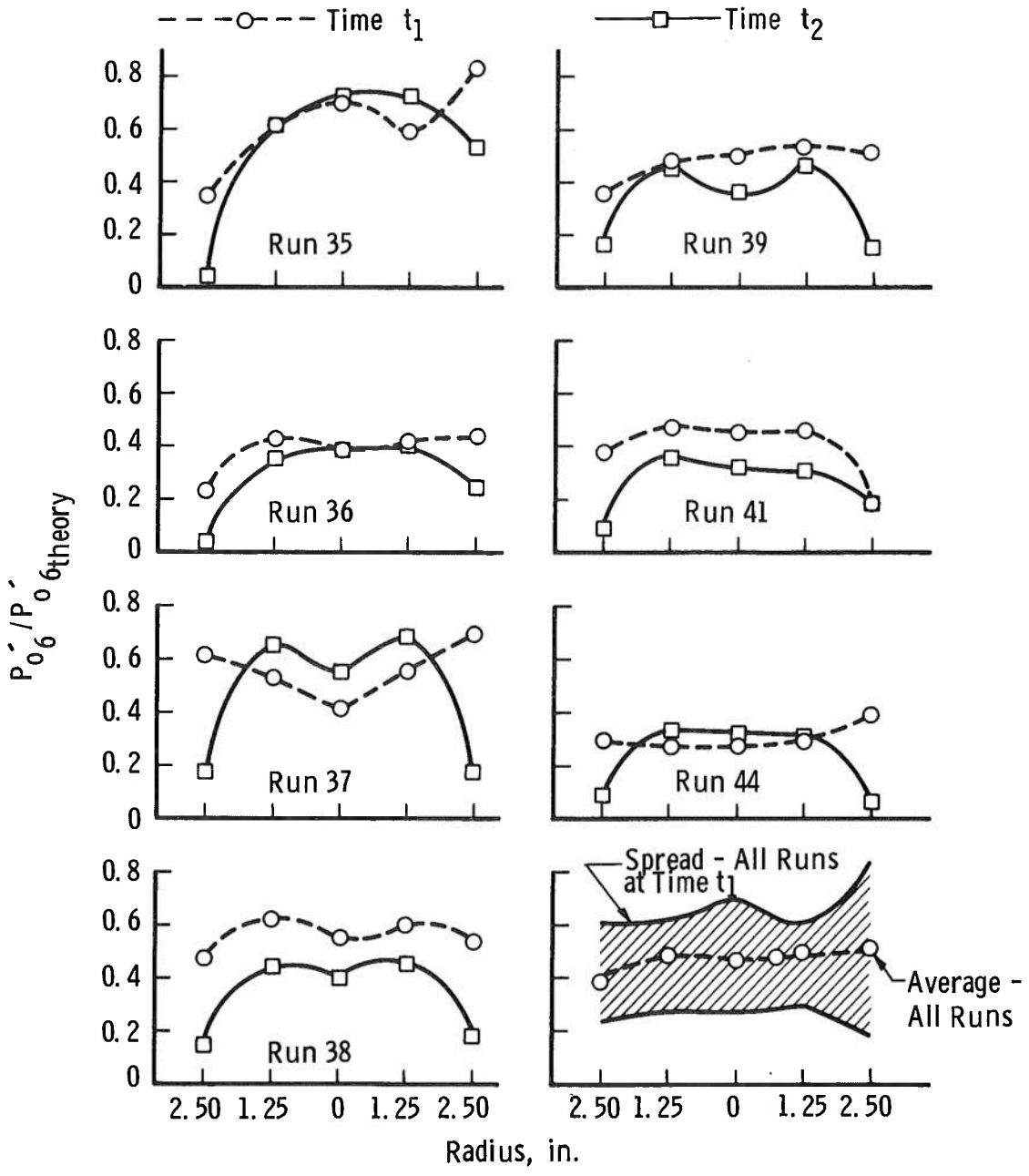

Fig. 32 Pitot Pressure Profile – Modified Expansion Tube

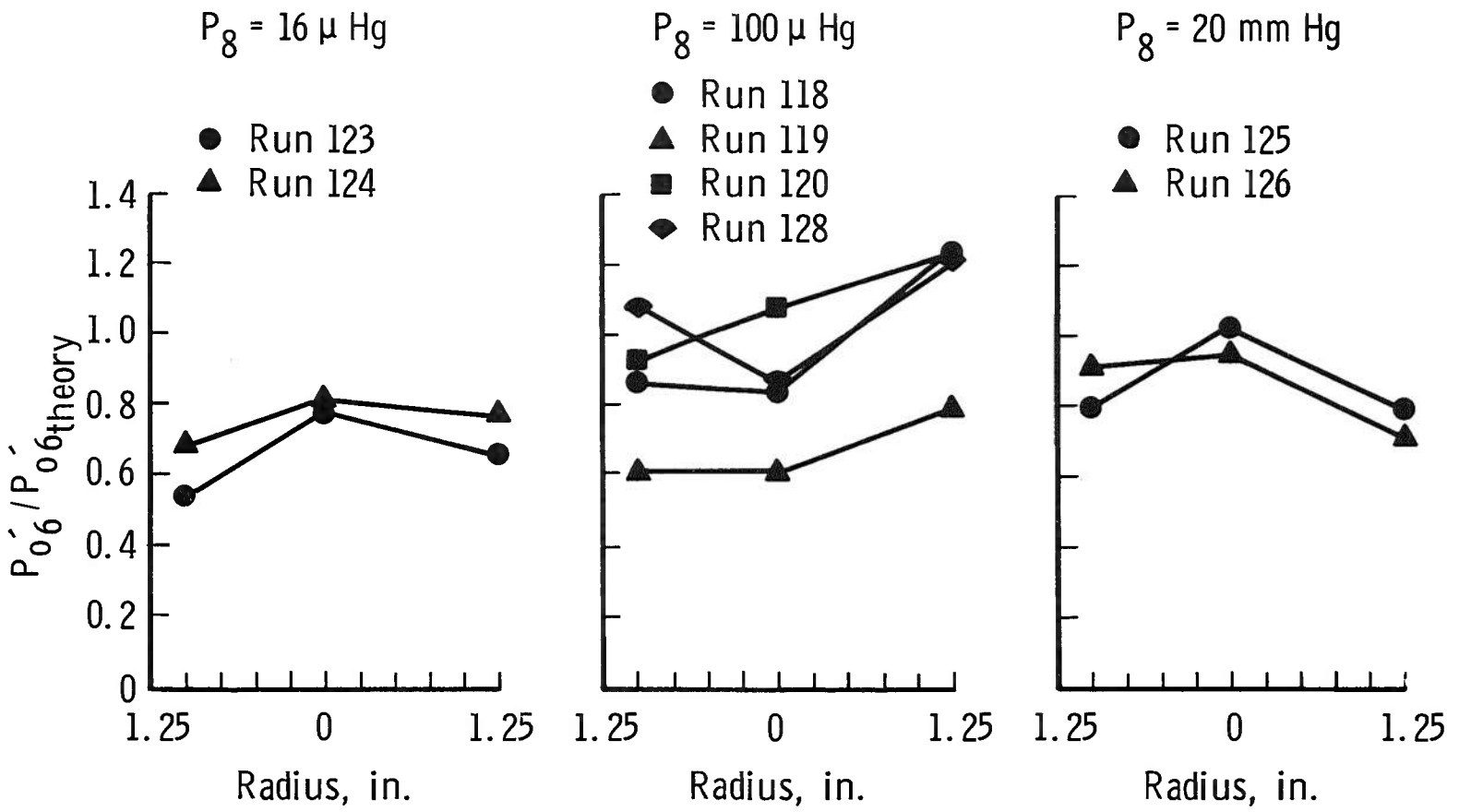

Fig. 33 Pitot Pressure Profile – High Density Shock Tube

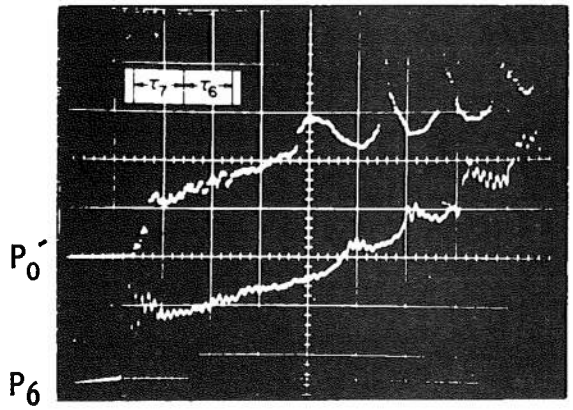

Run 155
P_8 = 18 μ Hg

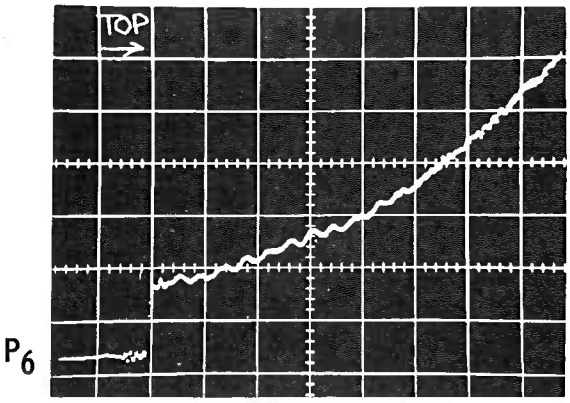

Run 126
P_8 = 18 mm Hg

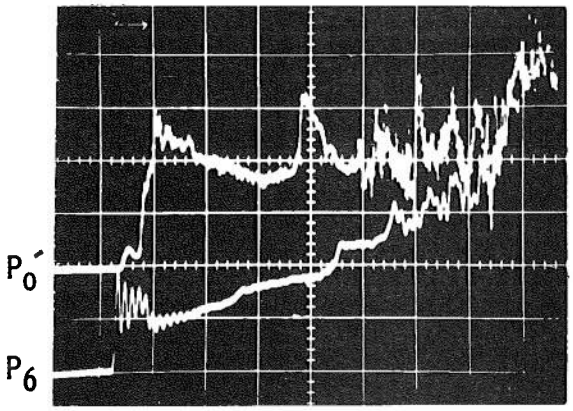

Run 153
P_8 = 18 μ Hg

Modified Expansion Tube

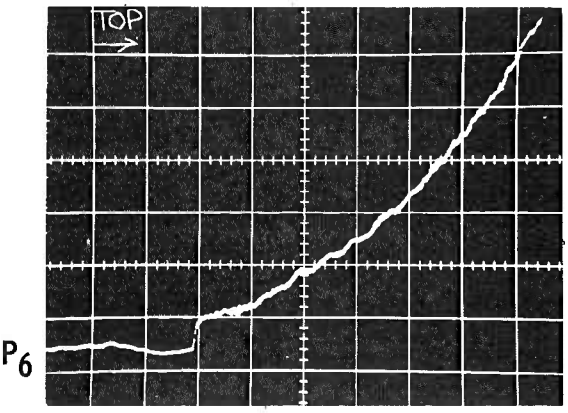

Run 114
P_8 = 2.8 mm Hg

High Density Shock Tube

Sweep Rate 200 μ sec/cm

Fig. 34 Static Pressure Measurements

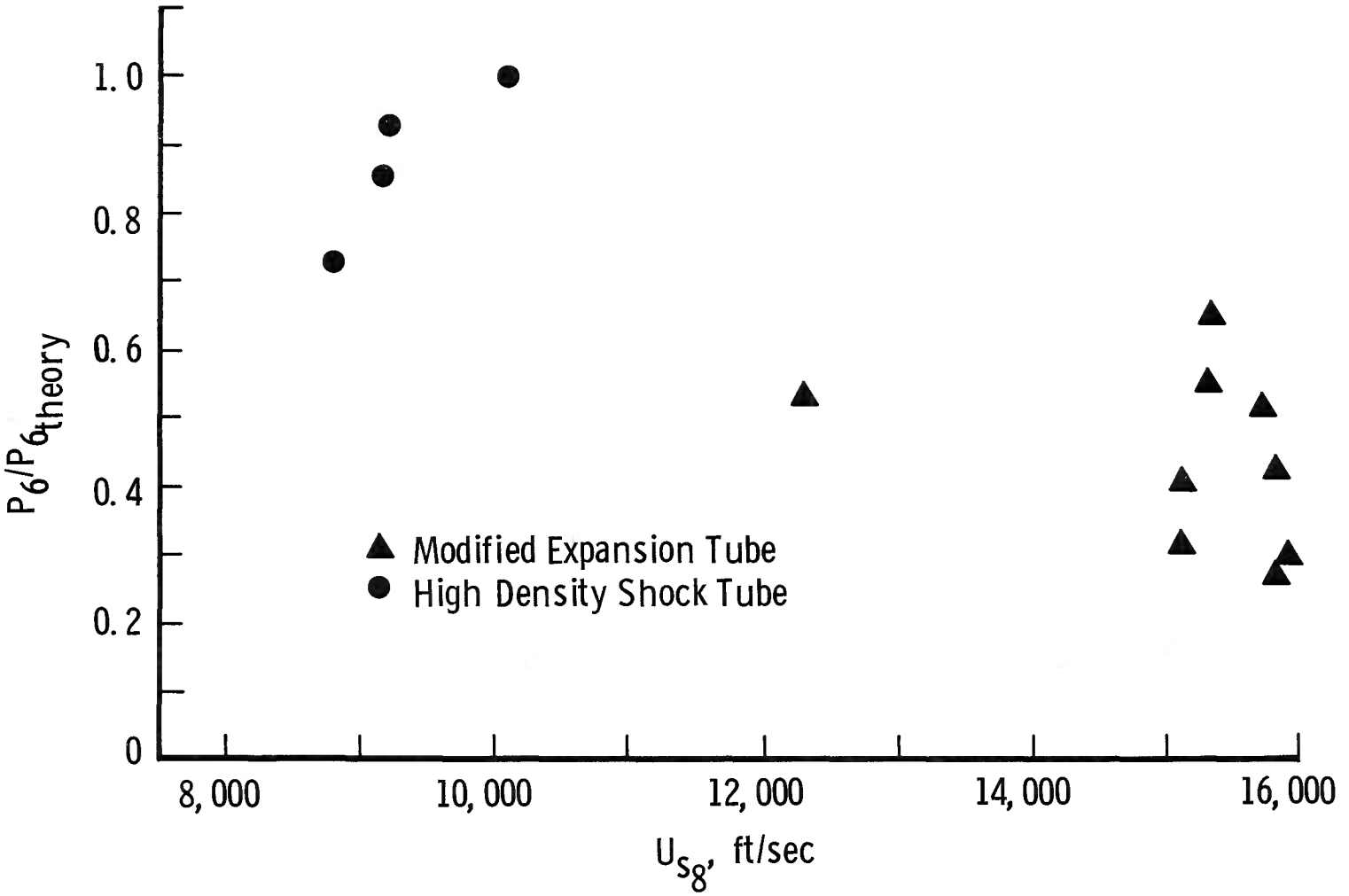

Fig. 35 Wall Static Pressure at the Test Section

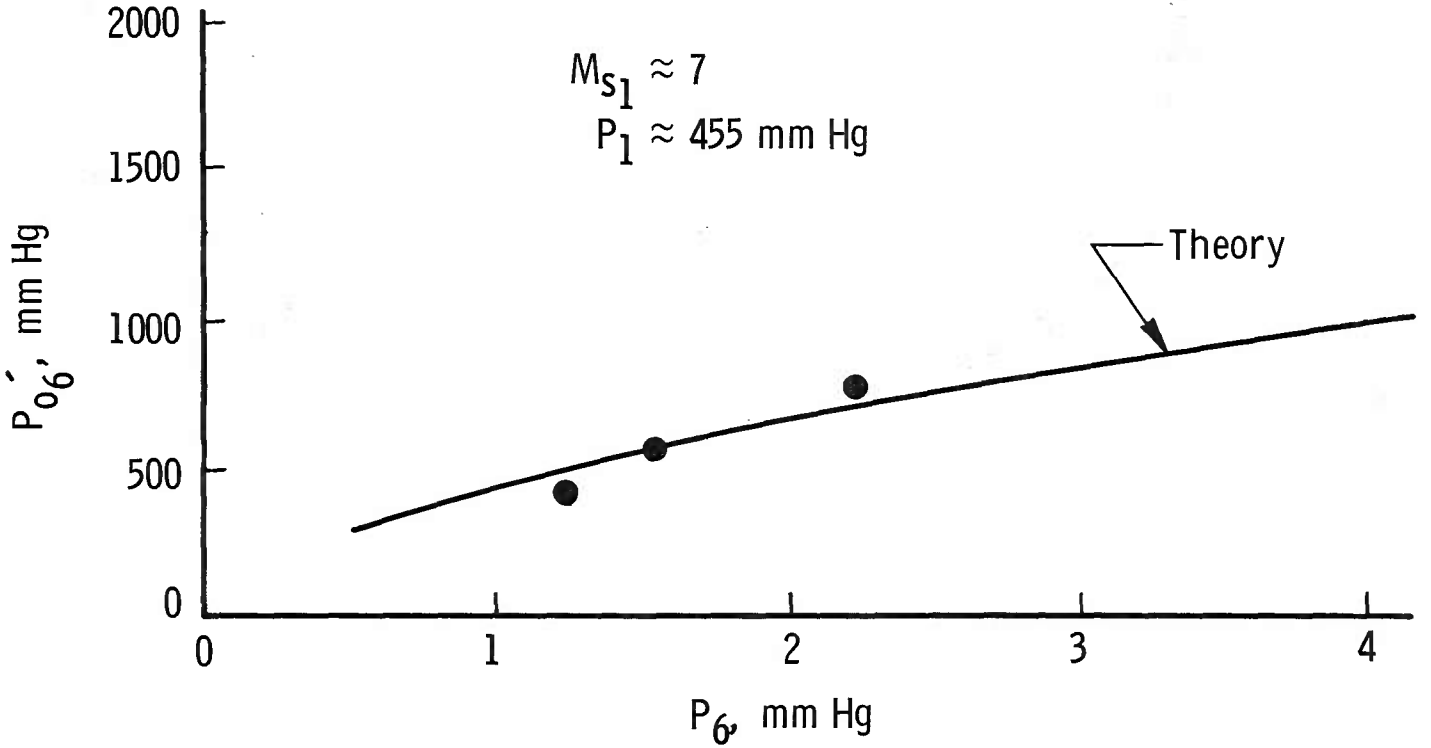

Fig. 36 Measured Pitot and Wall Static Pressure Compared with Theory-Modified Expansion Tube

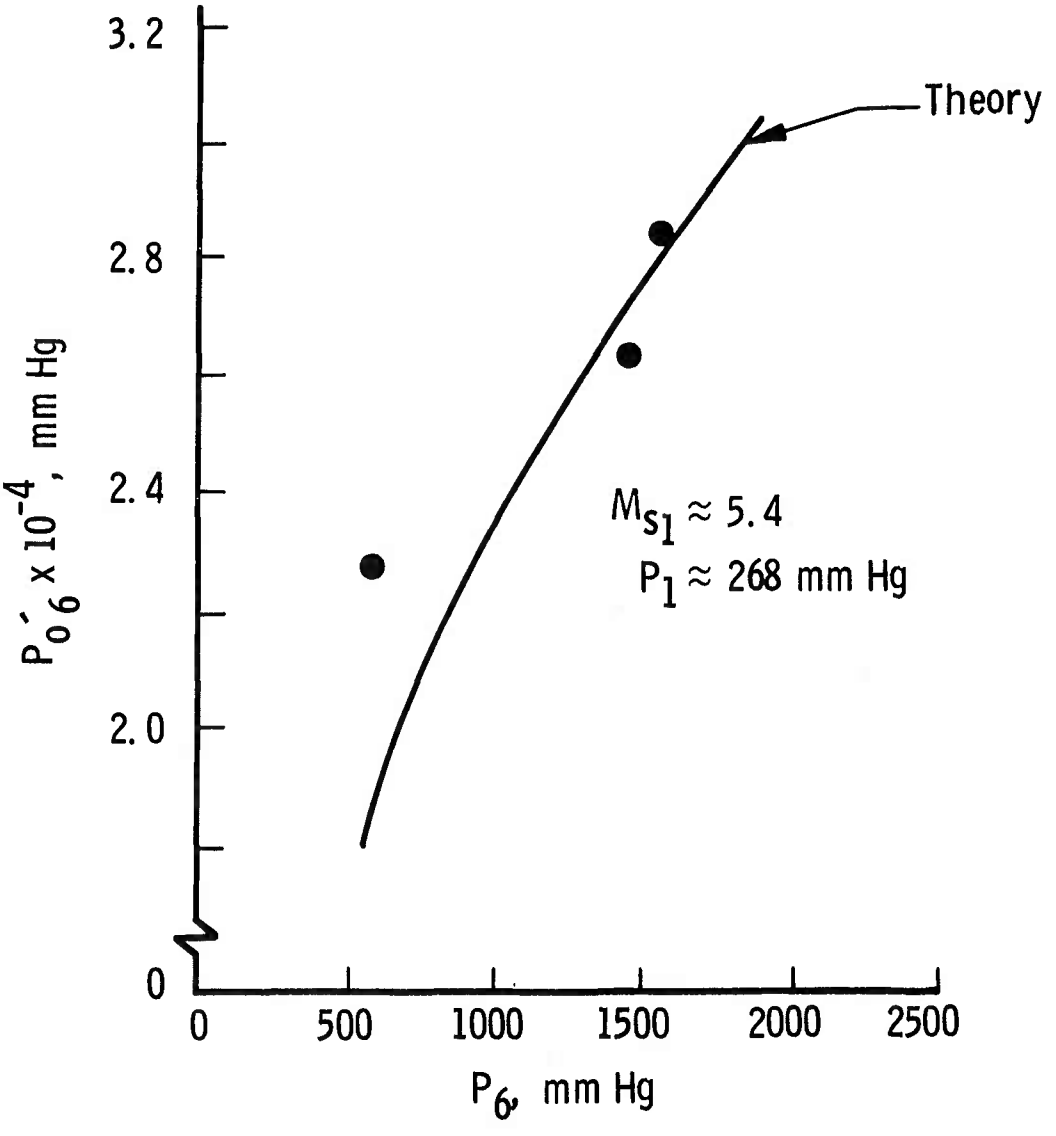

Fig. 37 Measured Pitot and Wall Static Pressure Compared with Theory – High Density Shock Tube

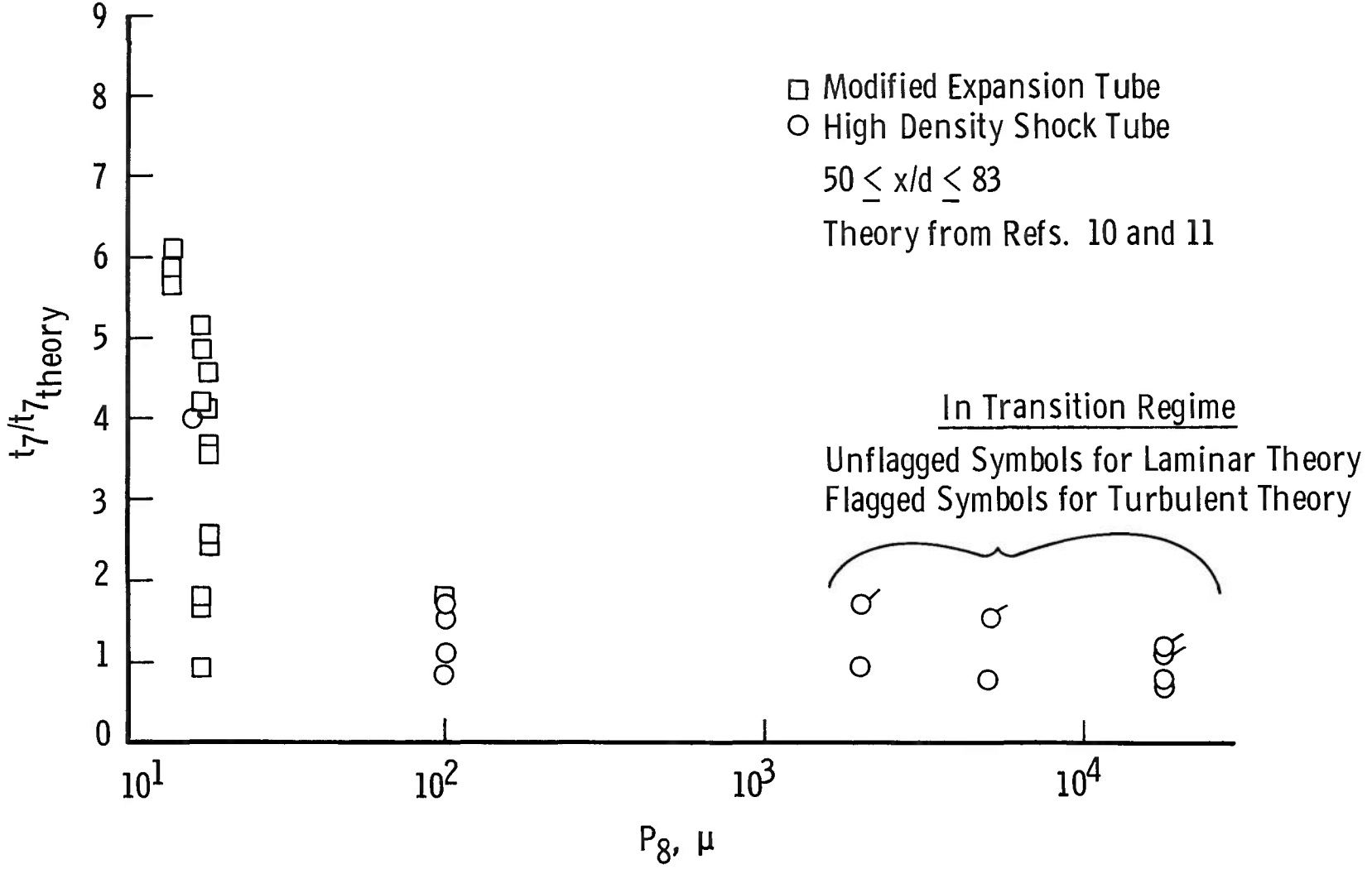

Fig. 38 Shock Heated Gas Passage Time, t_7

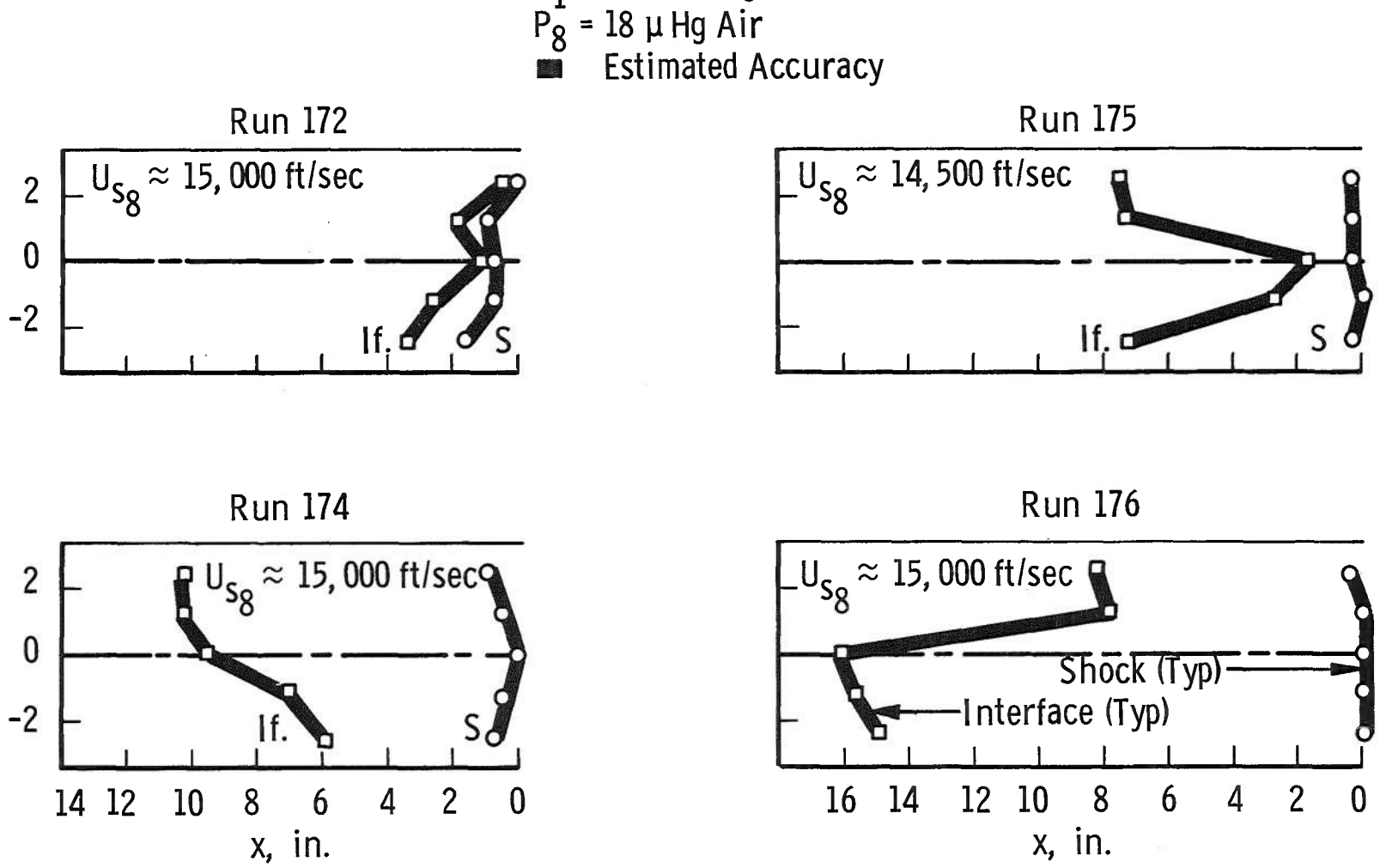

Fig. 39 Shock-Interface Separation

TABLE I
INSTRUMENTATION

Measurement	Range	Strain-gage pressure transducer	Sensitivity	Rise Time	Filter	Readout	Est. Accuracy
I. P_4	5-25 K psi	Strain-gage pressure transducer	---	Steady state	---	Millivolt recorder	±10%
II. P_1	4-9 psia	Aneroid barometer	---	Steady state	---	Visual	±1%
III. P_8	15μHg - 5 psia	Thermocouple, McLeod and aneroid barometer	---	Steady state	---	Visual	±10% or less
IV. P_2	100-500 psia	Piezoelectric	7 mv/psi	5 μsec	100 kc low pass	Oscilloscope	±10%
V. P_6	0.04-200 psia	Variable-capacitance and piezoelectric	500 mv/psi 7 mv/psi	15 μsec 5 μsec	100 kc notch 100 kc low pass	Oscilloscope	±17%
VI. P'_{0_6}	6-700 psia	Piezoelectric	7 mv/psi or 0.7 mv/psi	5 μsec	100 kc low pass	Oscilloscope	±12%
VII. U_{S_1} U_{S_8}	5000-8000 fps 5000-16,000 fps	Platinum thin film	---	< 1 μsec	---	Raster Oscilloscope	±3%

TABLE II
"SPIKE" HYPOTHESES

Hypothesis	Parameter	Variation
I. Mechanically induced accelerations	Model and model support system	All models of Fig. 11, single pitot probe supported from tube wall, pitot rake supported from "isolated" dump tank, sting length varied.
II. Instrumentation difficulties	Pressure transducer and associated circuitry	Instrumentation used in the centerline probe of pitot rake exchanged with that used in an off-center probe.
III. Flow instability on model	Model configuration	1.4-in.-diam. flat-face cylinder 0.3-in.-diam. flat-face probe 2-in.-diam. hemisphere-cylinder
IV. Oblique shock from wall	Longitudinal location of model	$18 \leq \ell_8 \leq 46$ ft
V. Accelerating tube viscous effects	Accelerating tube charge gas	$p_{He + Air}$ = 30 Hg, 40, 60, 100 } $p_{air} = 10 \mu Hg$
VI. Secondary diaphragm rupture effects	Secondary diaphragm thickness and material	1 and 2 1/4 mil polyester 1 to 8 3/4 mil polyester 1 1/4 mil aluminum coated polyester 1 3/4 mil aluminum foil
VII. Flow contamination by secondary diaphragm	(Same as VI)	(Same as VI)
VIII. Area change effect	Area ratio	A_{8_1} = 1.0 and 18.3

UNCLASSIFIED

Security Classification

DOCUMENT CONTROL DATA - R&D

(Security classification of title, body of abstract and indexing annotation must be entered when the overall report is classified)

1. ORIGINATING ACTIVITY *(Corporate author)*
Arnold Engineering Development Center
ARO, Inc., Operating Contractor
Arnold Air Force Station, Tennessee

2a. REPORT SECURITY CLASSIFICATION
UNCLASSIFIED

2b. GROUP
N/A

3. REPORT TITLE
RESULTS OF AN EXPERIMENTAL INVESTIGATION OF THE PERFORMANCE OF AN EXPANSION TUBE

4. DESCRIPTIVE NOTES *(Type of report and inclusive dates)*
N/A

5. AUTHOR(S) *(Last name, first name, initial)*
Glenn D. Norfleet, John J. Lacey, Jr., and Jack D. Whitfield, ARO, Inc.

6. REPORT DATE	7a. TOTAL NO. OF PAGES	7b. NO. OF REFS
February 1966	64	16

8a. CONTRACT OR GRANT NO.
AF40(600)-1200

b. PROJECT NO. 7778

c. Program Element 62410034

d. Task 777806

9a. ORIGINATOR'S REPORT NUMBER(S)
AEDC-TR-66-10

9b. OTHER REPORT NO(S) *(Any other numbers that may be assigned this report)*
N/A

10. AVAILABILITY/LIMITATION NOTICES
Qualified users may obtain copies of this report from DDC. Distribution of this document is unlimited.

11. SUPPLEMENTARY NOTES
N/A

12. SPONSORING MILITARY ACTIVITY
Arnold Engineering Development Center, Air Force Systems Command, Arnold Air Force Station, Tenn.

13. ABSTRACT

The results from an experimental study of an expansion tube conducted at the von Karman Gas Dynamics Facility (VKF) are presented and discussed. The research was conducted in two facilities: (1) a 6.75-in.-diam Modified Expansion Tube (MET) which utilizes a partially steady and partially unsteady expansion process, and (2) a 4-in.-diam (constant diameter) High Density Shock Tube (HDST) operated in an expansion tube mode for a completely unsteady expansion of the shock-heated gas to the final test condition. Flow velocities from approximately 9000 to 16,000 ft/sec were studied. The theoretical performance of expansion tubes in terms of velocity is found to be nearly obtained; however, the steadiness of the resulting flow leaves much to be desired, and the definition of accurate flow conditions remains in serious doubt.

DD FORM 1 JAN 64 1473

UNCLASSIFIED

Security Classification

14. KEY WORDS	LINK A		LINK B		LINK C	
	ROLE	WT	ROLE	WT	ROLE	WT
Expansion tubes						
Shock tubes						
Velocity						
Performance						
Pitot pressure						
Static pressure						
Hypervelocity flow						
Test devices						

INSTRUCTIONS

1. ORIGINATING ACTIVITY: Enter the name and address of the contractor, subcontractor, grantee, Department of Defense activity or other organization *(corporate author)* issuing the report.

2*a*. REPORT SECURITY CLASSIFICATION: Enter the overall security classification of the report. Indicate whether "Restricted Data" is included. Marking is to be in accordance with appropriate security regulations.

2*b*. GROUP: Automatic downgrading is specified in DoD Directive 5200.10 and Armed Forces Industrial Manual. Enter the group number. Also, when applicable, show that optional markings have been used for Group 3 and Group 4 as authorized.

3. REPORT TITLE: Enter the complete report title in all capital letters. Titles in all cases should be unclassified. If a meaningful title cannot be selected without classification, show title classification in all capitals in parenthesis immediately following the title.

4. DESCRIPTIVE NOTES: If appropriate, enter the type of report, e.g., interim, progress, summary, annual, or final. Give the inclusive dates when a specific reporting period is covered.

5. AUTHOR(S): Enter the name(s) of author(s) as shown on or in the report. Enter last name, first name, middle initial. If military, show rank and branch of service. The name of the principal author is an absolute minimum requirement.

6. REPORT DATE: Enter the date of the report as day, month, year; or month, year. If more than one date appears on the report, use date of publication.

7*a*. TOTAL NUMBER OF PAGES: The total page count should follow normal pagination procedures, i.e., enter the number of pages containing information.

7*b*. NUMBER OF REFERENCES: Enter the total number of references cited in the report.

8*a*. CONTRACT OR GRANT NUMBER: If appropriate, enter the applicable number of the contract or grant under which the report was written.

8*b*, 8*c*, & 8*d*. PROJECT NUMBER: Enter the appropriate military department identification, such as project number, subproject number, system numbers, task number, etc.

9*a*. ORIGINATOR'S REPORT NUMBER(S): Enter the official report number by which the document will be identified and controlled by the originating activity. This number must be unique to this report.

9*b*. OTHER REPORT NUMBER(S): If the report has been assigned any other report numbers *(either by the originator or by the sponsor)*, also enter this number(s).

10. AVAILABILITY/LIMITATION NOTICES: Enter any limitations on further dissemination of the report, other than those imposed by security classification, using standard statements such as:

(1) "Qualified requesters may obtain copies of this report from DDC."

(2) "Foreign announcement and dissemination of this report by DDC is not authorized."

(3) "U. S. Government agencies may obtain copies of this report directly from DDC. Other qualified DDC users shall request through _____."

(4) "U. S. military agencies may obtain copies of this report directly from DDC. Other qualified users shall request through _____."

(5) "All distribution of this report is controlled. Qualified DDC users shall request through _____."

If the report has been furnished to the Office of Technical Services, Department of Commerce, for sale to the public, indicate this fact and enter the price, if known.

11. SUPPLEMENTARY NOTES: Use for additional explanatory notes.

12. SPONSORING MILITARY ACTIVITY: Enter the name of the departmental project office or laboratory sponsoring *(paying for)* the research and development. Include address.

13. ABSTRACT: Enter an abstract giving a brief and factual summary of the document indicative of the report, even though it may also appear elsewhere in the body of the technical report. If additional space is required, a continuation sheet shall be attached.

It is highly desirable that the abstract of classified reports be unclassified. Each paragraph of the abstract shall end with an indication of the military security classification of the information in the paragraph, represented as *(TS)*, *(S)*, *(C)*, or *(U)*.

There is no limitation on the length of the abstract. However, the suggested length is from 150 to 225 words.

14. KEY WORDS: Key words are technically meaningful terms or short phrases that characterize a report and may be used as index entries for cataloging the report. Key words must be selected so that no security classification is required. Identifiers, such as equipment model designation, trade name, military project code name, geographic location, may be used as key words but will be followed by an indication of technical context. The assignment of links, rules, and weights is optional.